NAIST-IS-DD1361208

Doctoral Dissertation

Radio over Fiber based Wireless Access Technology for Flexible Channel Resource Allocation

Withawat Tangtrongpairoj

September 16, 2016

Department of Information Science
Graduate School of Information Science
Nara Institute of Science and Technology

A Doctoral Dissertation
submitted to Graduate School of Information Science,
Nara Institute of Science and Technology
in partial fulfillment of the requirements for the degree of
Doctor of ENGINEERING

Withawat Tangtrongpairoj

Thesis Committee:

Professor Minoru Okada	(Supervisor)
Professor Shoji Kasahara	(Co-supervisor)
Associate Professor Takeshi Higashino	(Co-supervisor)
Assistant Professor Yafei Hou	(Co-supervisor)

Radio over Fiber based Wireless Access Technology for Flexible Channel Resource Allocation*

Withawat Tangtrongpairoj

Abstract

Radio over Fiber (RoF) with the centralized radio access network (C-RAN) is a promising solution for providing wireless access services. Heterogeneous radio signals are transferred via an optical fiber link using the digital or analog transmission techniques. Since the analog RoF has many advantages such as the link bandwidth utilization and low complexity, this thesis comprises multiple studies to conclude the performance of analog RoF not only for the network-level but also the link-level. We could successfully introduce a very simple and easy-to-use solution adaptation technique, whose performance was shown to be outstanding. Firstly, we have considered the performance of network-level improvement using the C-RAN with analog RoF. The mobile backhaul and fronthaul are capable of deploying the cells at the indoor location. However, since its link topology is based on the point-to-point, the handover process must be activated whenever the mobile user moves across the cell. As for the indoor system, the number of handover is further increased than outdoor location because of the limitation of transmitting power of the indoor equipment. In this research, C-RAN incorporated with optical matrix switch is introduced instead of the point-to-point link. Simulation results show that the proposal reduces a huge number of handover compared to the conventional point-to-point configuration. Then, as a continuation study for the link-level, when the analog RoF and the radio

*Doctoral Dissertation, Department of Information Science, Graduate School of Information Science, Nara Institute of Science and Technology, NAIST-IS-DD1361208, September 16, 2016.

frequency (RF) devices have a nonlinear characteristic, these will create the intermodulation products (IMPs) in the system and generate the intermodulation distortion (IMD). In this research, the IMD interference in the uplink RF signals from the coupling effect between the downlink and the uplink antennas has been addressed. We propose a method using the dynamic channel allocation (DCA) algorithm with the predistortion (PD) technique to improve the throughput performance of the multi-channel RoF system. The carrier to distortion plus noise power ratio (CDNR) is evaluated for all channel allocation combinations; then the best channel combination is assigned as a set of active channels to minimize the effect of IMD. The results show that the DCA with PD has the lowest IMD and obtains a better throughput performance.

Keywords:

Radio over Fiber, Centralized radio access network, Wireless network, Handover, Dynamic channel allocation, Predistortion, Nonlinearity

Acknowledgements

This dissertation would not have been finished without the people who had supported me wholeheartedly. First and foremost, I would like to thank my supervisor Professor Minoru Okada, who always supported me, not only my researches but also all my life during my stay in Japan. For the first time I came here, I had no experience about the physical layer. He taught me always to focus on whole layers of the network; every layer has their own responsibility. His advice he gave me on the day I started my Ph.D. life has become one of my most prized pieces of advice in my life. I really appreciated that. To Associate Professor Takeshi Higashino, my adviser, who introduced me to the Radio over Fiber communication system. I appreciate his patient on me when I completely had almost zero knowledge about the Radio over Fiber. Without the opportunity he gave me on that day, this thesis could not be finished. To my thesis committee, I would like to thank Professor Shoji Kasahara, who have seen my work in my final defense. His advice during the presentation inspired me a lot of new ideas and drive on my new research. I really appreciated that. To Assistant Professor Yafei Hou, his kindness and patience has put me at ease and made my journal paper good enough to be published. I am thankful to him for all his advice. To Assistant Professor Duong Quang Thang, your morale has always light me up from the dark. To all Network System Lab members, I would like to thank for all of your friendship. Special thanks to Hayashi-san for her kindly supports and helping. To Associate Professor Anan Phonphoem, he is like my father. He taught me not only how to do the research, but also how to be the good man. I would say that my successful of my life is because of him. Also, I would like to thank Nara Institute of Science and Technology for granting me the greatest scholarship, which supported my allowance during the Ph.D. life here in Japan. Finally and most importantly, I dedicate this dissertation to my family and my girlfriend. I am grateful to them for allowing me to catch my dream.

To my family,
forever thankful for their love, endless support and sacrifice

List of Publications

Peer review journal paper

1. Withawat Tangtrongpairoj, Yafei Hou, Takeshi Higashino, and Minoru Okada, "Quality-based Channel Allocation Scheme with Predistortion in Multi-channel Radio over Fiber System", IEICE Transactions on Electronics, Vol.E99-C, No.5, pp.563-573, May. 2016.

Peer review journal letter

1. Withawat Tangtrongpairoj, Takeshi Higashino, and Minoru Okada, "Handover Reduction using Optical Matrix Switch for Indoor LTE Cell Deployment", IEICE Communication Express (ComEX). doi:10.1587/comex.2016XBL0151

Peer review international conferences

1. Withawat Tangtrongpairoj, Takeshi Higashino, and Minoru Okada, "Performance Evaluation of Multi-Channel RoF using Radio Frequency Allocation," In Proceedings of the 19th European Conference on Networks and Optical Communications (NOC), pp.80-85, Jun. 2014.

2. Withawat Tangtrongpairoj, Takeshi Higashino, and Minoru Okada, "Quality-based Channel Allocation Scheme in Multi-channel Radio-over-Fiber System," In Proceedings of the 30th International Technical Conference on Circuits/Systems, Computers and Communications (ITC-CSCC), pp.752-755, Jul. 2014.

3. Withawat Tangtrongpairoj, Takeshi Higashino, and Minoru Okada, "Quality-based Channel Selection in Multi-channel Radio-over-Fiber System," In Proceedings of the Asia-Pacific Signal and Information Processing Association Annual Summit and Conference (APSIPA), pp.1-5, Dec. 2014.

4. Withawat Tangtrongpairoj, Takeshi Higashino, and Minoru Okada, "Handover Reduction among indoor LTE Cells for Centralized-RAN," In Proceedings of the International Workshop on Smart Info-Media Systems in Asia (SISA), pp.43-47, Sep. 2016.

Workshops

1. Withawat Tangtrongpairoj, Takeshi Higashino, and Minoru Okada, "Quality-based Channel Allocation Scheme with Pre-distortion in Multi-channel Radio-over-Fiber System", IEEE Communications Society, Kansai Chapter (ComSoc), COM14-5, Oct. 2014.

2. Withawat Tangtrongpairoj, Takeshi Higashino, and Minoru Okada, "A Performance Comparison of Load Balancing among Radio-over-Fiber Indoor LTE Small Cells", Photonics-applied Electromagnetic Measurement International Workshop (PEM), Vol.1, No.1, FCA-10, Nov. 2015.

3. Withawat Tangtrongpairoj, Takeshi Higashino, and Minoru Okada, "Handover Reduction using Optical Matrix Switch for Centralized Radio Access Network ", IEICE Smart Info-media System (SIS), pp.65-68, Sep. 2016.

Contents

List of Figures

List of Tables

Chapter 1

Introduction

1.1. Overview

The increasing popularity of mobile devices fosters technological advancement in wireless communication. Nowadays, tablets and mobile devices are equipped with different types of wireless modules. This will create problems such as interference and bandwidth expansion, given the larger bandwidth requirements of the multimedia services. To support the growing traffic of heterogeneous wireless air interfaces, the Radio over Fiber (RoF) with centralized radio access network (C-RAN) has been deployed. The main purpose of the C-RAN is to separate the baseband unit (BBU) from the remote antenna unit (RAU) and merge the function of BBU into the centralized control station (CCS). Furthermore, the configuration between the RAU and the CCS can be simplified by introducing the RoF link. The RoF can be categorized into two configurations: digitized RoF and analog RoF. To make the RAU simple and to support the next generation of the communication system, we proposed to use the analog RoF with the C-RAN configuration for all of the parts of this thesis. According to RoF configuration, the radio frequency (RF) signal modulates the optical carrier and transmits it over the optical fiber link as the analog waveform. At the RAU, an antenna is located for radiating the downlink radio signals and receiving the uplink radio signals. Although they are deployed separately, these antennas can often be combined for radiating and receiving by using a circulator device. Since the RAU using fiber-optics has a larger bandwidth than the coaxial cable and the radio link, the different kinds of RF signals can be simultaneously transported. Additionally, the fiber-optic cable is capable of distributing the optical signals with low loss; therefore, the CCS can receive different types of signals simultaneously, given that there is an RF transceiver for each signal. The RF channel control module can select carrier frequencies for the connecting RF transceiver. In this thesis, we divided our researches into two parts: network-level and link-level performance enhancement.

In parts of network-level, mobile backhaul link for constructing the small cell network is composed of the BBU and RAU, and these are connected by RoF. It can be considered that the above optical link contributes for deploying small cell in the indoor location. One problem in deploying radio coverage in indoor location is that cell size must be smaller than outdoor location, because of the presence of larger number of the obstacle compared to outdoor location and limited transmitting power of indoor equipment. Since the conventional RoF and Ethernet link are based on the point-to-point link, it is anticipated that handover process between cells often occurs in operation, that is, processing data stream in a BBU is required to switch to the other one whenever mobile terminal moves across beyond the currently connected cell.

In parts of link-level, the type of interference commonly found in the analog RoF using nonlinear devices is intermodulation distortion (IMD), which is produced when heterogeneous signals are simultaneously transmitted. In the previous study [1], it is demonstrated that both the 2.4 GHz band and the 5 GHz band WiFi signals can be transported over the RoF link without any critical quality degradation of the uplink and the downlink throughput performance. In the WiFi system, a different number of channels is allocated depending on the frequency band: 14 channels for the 2.4 GHz, 4 channels for the 5.2 GHz and 11 channels for the 5.6 GHz bands [2]. The differing number of channels is regarded as a multi-channel WiFi commonly used in a communication system. However, their performance has not yet been investigated even though this problem of the IMD remains unsolved in the research.

Our studies for the past 3 years composing into this thesis has been aimed to improve the quality of the RoF not only for network-level but also in the link-level. We first discussed about the handover reduction using the optical matrix switch instead of the point-to-point connection. Since the waveform format is analog, one optical stream is easily distributed to multiple remote sites by dividing it passively. Therefore, radio resource in one BBU can be shared among multiple cells. Furthermore, we also propose the algorithm which is implemented in the optical matrix switch. In our algorithm, the neighboring RAUs which are located close together will be grouped to the same BBU. Hence, the reduction of the BBU can be observed accompany with the decreasing of the handover. Since the analog RoF is deployed, the nonlinear characteristic occurs and generates the IMD in the system. The second part of this thesis proposed a method using the dynamic channel allocation (DCA) algorithm with the predistortion (PD) technique which aims to reduce the IMD in the link-level. Our improvement to the method was evaluated by using the carrier to distortion plus noise power ratio (CDNR). From the results of using the DCA with the PD, the optimal transmission power can be obtained. Moreover, we confirm that our proposal can improve the throughput performance in the realistic WiFi by using the network simulation.

1.2. Contributions

The contributions of the studies composing into this thesis are mainly in two-fold:

- In the first part, **we introduce the new mobile fronthaul configuration using the optical matrix switch for control the connection between the BBUs and the RAUs**, which a cell where a large number of mobile terminals exist is combined with several neighboring cells, then handover is no longer required at combined cell even though the mobile terminal move out of the cell. As the secondary advantage of radio resource sharing among cells, required number of BBUs in CCS can be reduced. The performance evaluation including the number of handovers and the required number of BBUs are reported in Chapter 3.

- The second part of this thesis focuses on the performance of the system considering the nonlinearity when the multi-channel WiFi signals are simultaneously transmitted. **The problem of IMD interference between the uplink and the downlink radio signals in a multi-channel RoF**

system has been addressed in this work, since it has not been reported to date. This kind of IMD interference occurs when a media access is controlled independently in each frequency-division multiplex radio signal. In the 5 GHz WiFi system, all channels are independent and its carrier-sense multiple access (CSMA) is also carried out independently of each other. Since the uplink and downlink signals are asynchronously transmitted in a channel, the transmitted signals can cause IMD in neighboring channels under the presence of antenna coupling. **The main contribution of this part is to introduce two methods for nonlinear compensation: DCA and PD** as shown in Chapter 4. Regarding DCA, the CDNR is evaluated for all possible combinations for determining the active channels. We then assign, as the active channels, the best channel combination, i.e. that which has the highest average CDNR that minimizes the effect of IMD. Simulated results show that the CDNR performance in the DCA deteriorates drastically when the number of active channels is more than 4. Therefore, a combination of the DCA and the PD is proposed to achieve better performance.

1.3. Structure of this Thesis

This thesis is structured as follows: Chapter 2 shares common materials on background notes of RoF and C-RAN. This chapter explains the general concept of the RoF and its components, which are the E/O, fiber, O/E, common public radio interface (CPRI), power amplifier (PA). The research studies of this thesis begin in Chapter 3, where we proposed the handover reduction algorithm for controlling the optical matrix switch. Moreover, not only for network-level but also link-level, we investigated the nonlinear uplink problem and proposed the methods to solve IMD in Chapter 4. The conclusion of this thesis is shown in Chapter 5.

Chapter 2

Radio over Fiber and Centralized Radio Access Network for Mobile Communications

Chapter 2 explains the common materials that are shared by later chapters. In this chapter, we mainly focus on the general concept of the Radio over Fiber (RoF) and centralized radio access network (C-RAN) communication. For details related to the evaluation procedures, such as handover reduction, dynamic channel allocation (DCA), and predistortion (PD) they will be explained in the next chapter. All these materials are presented upfront to avoid repeating of the information as many later chapters frequently refer to these materials. For a more specific background that may be only required by an individual chapter, we will provide them later in those chapters.

2.1. Background of Radio over Fiber (RoF)

RoF was first proposed in 1990 to serve the increasing bandwidth demand [3]. Since that time, many researchers try to improve the performance of the RoF, which many field trials have been performed.

The RoF is proposed as the fiber-optic waveform transmission without any intentionally required change of the original signal. The signal is modulated with the light source which has two major features as follows. The first feature is

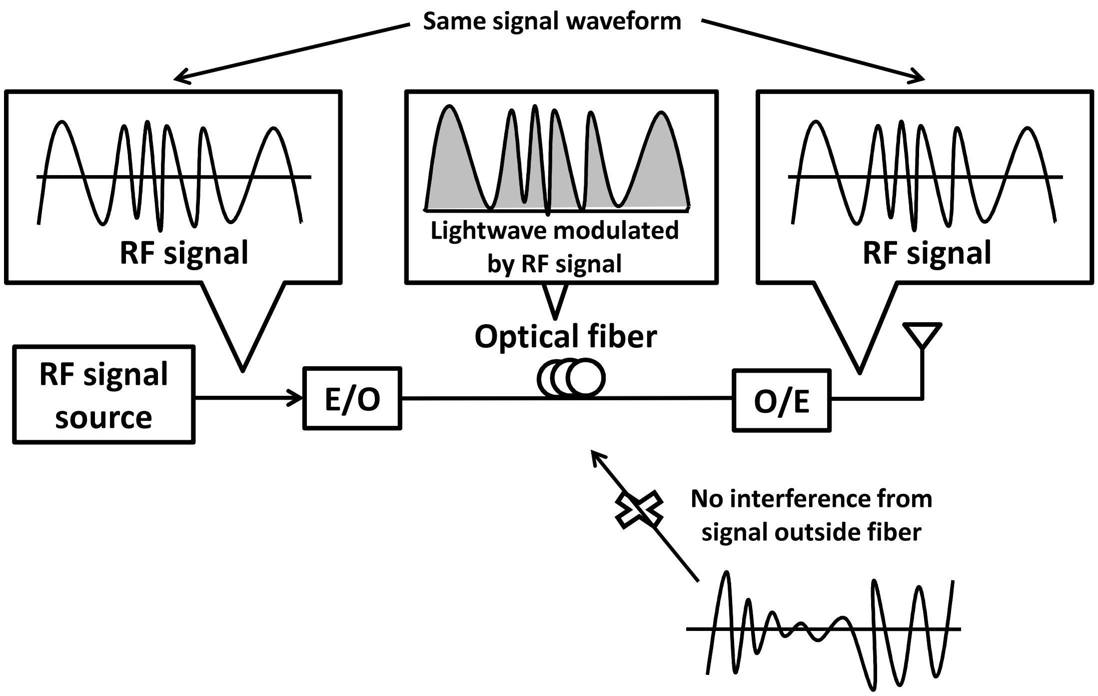

Figure 2.1. RoF basic transmission

RoF signals in the fiber have no interference from the radio signal outside of the fiber. The second is the waveform of the radio frequency (RF) signal is essentially conservation during the fiber-optic transmission, which means the signal before and after optical fiber must be the same. These characteristics are shown in Fig. 2.1 [4]. However, due to the long distance of the fiber transmission (10 km), we considered the loss of the fiber-optic as will explain in Chapter 4.2. As the present, RoF can be classified into two types: the **analog RoF** and the **digitized RoF**. RoF is basically an analog transmission system because the radio waveform can be directly distributed at the radio carrier frequency, from the centralized control station (CCS) to the remote antenna unit (RAU). The details of the RoF are shown in the later sections. However, it is better to compare the analog RoF with digitized RoF regarding to their advantages.

Fig. 2.2 shows the configuration of analog RoF. In the downlink, the data stream modulated with baseband and upconverter, which results in RF signal. Then, the RF signal is transported in an analog format over the fiber-optic to

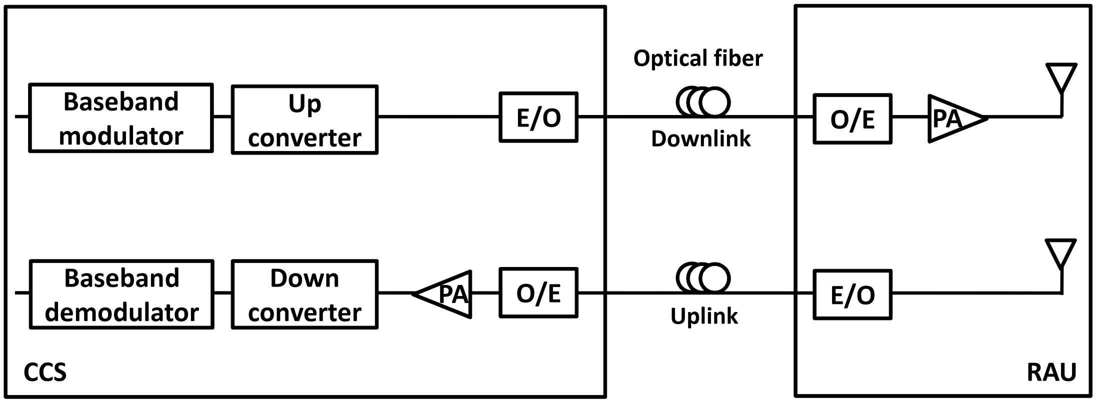

Figure 2.2. Analog RoF

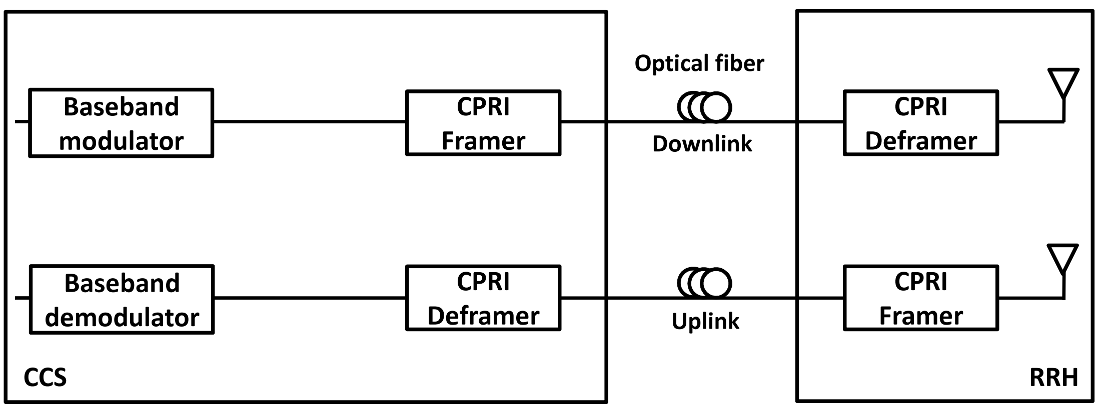

Figure 2.3. Digitized RoF

the RAU, noted that the modulated and demodulated RF devices to the optical domain are electrical to optical converter (E/O) and optical to electrical converter (O/E), respectively. From this architecture, the RAU can be simplified to a simple node by processing as only the antenna function and optical converter, which is flexible regarding where it can be installed. However, the most of the problems that can be easily found are the nonlinearity from optical devices and the noise tolerance of the analog transmission.

By incorporating the digitized RoF system, all basic analog parts are replaced by digital equipment, which results in scalability, energy efficiency, and

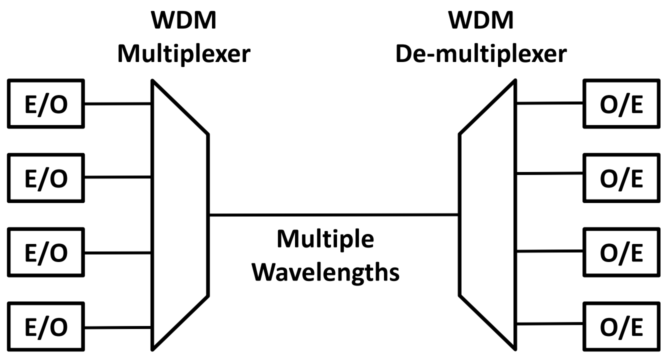

Figure 2.4. Analog RoF with WDM

low implementation cost. Hence, the problems of nonlinearity and noise tolerance can be neglected. The remote radio head (RRH) is deployed at the cell site. The common public radio interface (CPRI) is widely used for the digitized RoF. From Fig. 2.3, in the CPRI framer, the IQ data from the baseband modulator is transformed to the digital signal by using analog to digital converter (ADC), then transmits to the optical transmission using the time division multiplexing as shown in subsection 2.1.4. Moreover, many functions are implemented in CPRI framer and deframer, such as ADC, digital to analog converter (DAC), upconverter, downconverter, power amplifier and low noise amplification as shown in Table 2.2. The transmission rate of the CPRI links increases with the number of sectors, number of antennas for each sector and the bandwidth of transmitted signal. For example, when using 20 MHz Long Term Evolution (LTE) signal with a single sector and two antennas with multiple-input multiple-output (MIMO), the CPRI transmission rate is about 2.458 Gbps [5].

Furthermore, assuming that three sectors with 16x16 MIMO with 20 MHz LTE-A signal are implemented, the required transmission rate is 100 Gbps [6]. Since the next generation of communication system required much higher bandwidth for the multi-band femtocell transmission, the enhancement of digitized RoF or new technologies must be considered. Many researchers try to propose many methods to deal with these challenges. Authors in [6] suggested to use IQ data compression for digitized RoF, but when the antennas and sectors increase, the bandwidth is still not enough. Another approach is to use the new technology which is the wavelength division multiplexing (WDM) [7] combining with the analog RoF. From Fig. 2.4, many wavelength channels are combined into one optical fiber using the WDM multiplexer. At the receiving site, WDM de-multiplexer is responsible for separate the wavelength, then pass the signal through the O/E. The results would enhance security and scalability to support the massive subscribers. In the ways that are easy to understand, we compare the pros and cons of the analog RoF and digital RoF in Table 2.1.

Table 2.1. Comparison between analog RoF and digitized RoF

	Nonlinearity	Base station	Complexity	Bandwidth utilization
Analog RoF	High	Simple	Low	High
Digitized RoF	Low	Complex	High	Low

Therefore, all of the chapters in this thesis use analog RoF, since the analog RoF is the key factor of the next generation of communication system. Fig. 2.2 and Fig. 2.3 show the components of the fiber-optic link consisting of E/O, optical fiber, O/E and CPRI. These four components are explained in the following subsections.

2.1.1 Electrical to Optical converter (E/O) or Optical transmitter

For the RoF, the principal purposes of the lasers are the wide range of applications, high-efficiency, and low-noise. The responsibility of the E/O is to modulate the RF signal with the light source using the laser diode. The atoms vibrate to perform a beam radiation by using the capability of the p-n junction [8], which all of the beam waves are the single wavelength with the same phase. The intensity of the laser light is explained by the light-current (L-I) curve as shown in Fig. 2.5. When the input current is higher than the threshold current (I_{TH}), the output of light power is increased as the linearity of the modulation gain (W/A). The efficiency of modulation depends on the manufacturing process, which the gain can be around 0.02 W/A to 0.3 W/A [9]. However, the use of fiber-optic transmitters are varied by the different kinds of applications, the exact model of these modules need to be carefully considered.

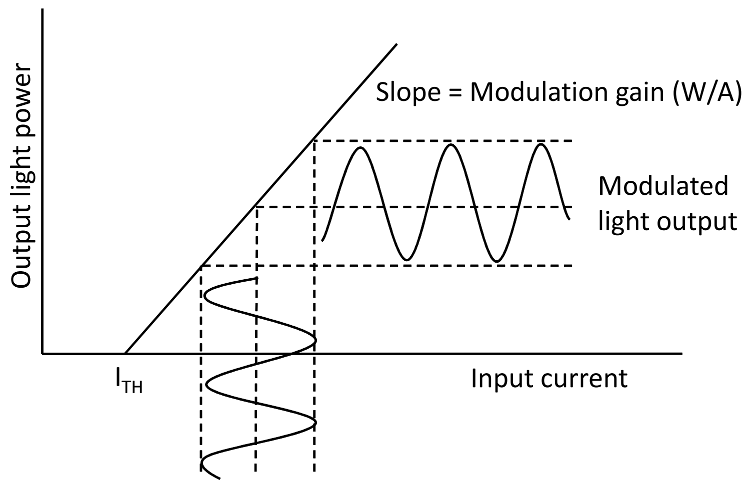

Figure 2.5. Input current and output power (L-I) curve

2.1.2 Fiber Optic Link

The fiber optic technology is mainly proposed for reducing cost and providing high reliable communication link since the light beam can transmit along with a thin glass. The glass or silica is surrounded by the cladding which is a medium that has a lower index of refraction. So, the light traveling in the core glass reflects from the cladding boundary. As a result, the fiber transmits all lights that enter the fiber to its destinations.

The optical fiber can be categorized into two groups: the single mode fiber (SMF) and the multi mode fiber (MMF). The key differences between these two types are the cost and distance. The SMF has much higher tolerances for practical use because the core is smaller, and the wavelength is narrower compared to the MMF. The core size of SMF and MMF are about 9 and 50 microns, respectively. From these effects, the MMF has a reach up to about 550 meters. However, the SMF has a greater distance which can run between 2 meters to 10,000 meters with a double of the cost.

Although, the fiber optic cables provide the superior performance of the communication system. However, due to the long distance of the links, some attenuations degrade the link quality, such as the loss from impurities, cladding, and wavelength. Due to these attenuations occur along with the fiber link, it is impossible to achieve the data rates up to 50 Gbps along with 100 kilometers of SMF without the need of an amplifier.

2.1.3 Optical to Electrical converter (O/E) or Optical receiver

At the end of the fiber-optic link, the light is detected by the O/E. The photodiode converts the light back to electrical current and distributes to its final destination. The key performance of the optical receiver is the photodiode itself, which the efficiency of the photodiode is given by the responsivity curve as shown in Fig. 2.6. The p-i-n diode was selected as the most common type to implement the photodiode. This type of diode provides the larger level of conversion than a p-n diode [9]. Moreover, specialized equipment such as optical isolator is also integrated to minimize the optical reflections from returning to the optical source [10].

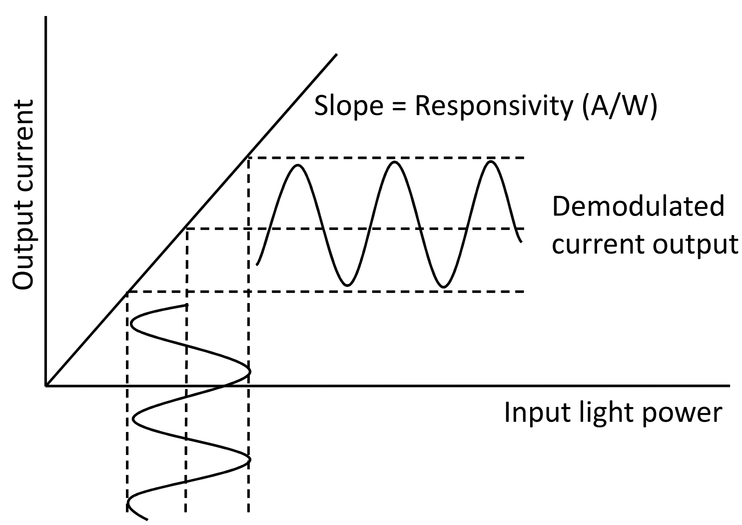

Figure 2.6. Photodiode linear responsivity curve

2.1.4 Common Public Radio Interface (CPRI) Protocol

CPRI protocol was proposed to enable the flexibility of RRH, according to where it can be installed. In another word, the purpose of CPRI is to allow RRH manufacturers to share a common protocol, which is easier to adapt platforms from one service provider to the other. There are many groups join on the defining CPRI specifications including Ericsson, Huawei Technologies, NEC Corporation, Nortel, Alcatel and Nokia Siemens Networks [11].

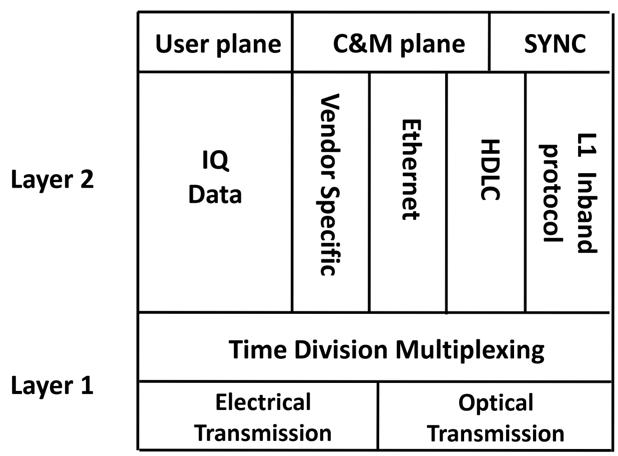

Figure 2.7. CPRI protocol

As for the Fig. 2.7, the user plane information is sent in the form of IQ data. The IQ data that came from the different RRHs are multiplex with a time division multiplexing scheme, then convert from electrical domain to optical domain. The control and management information (C&M) is sent by layer two protocols, which are high-level data link control (HDLC) and Ethernet. These protocols monitor and manage the IQ data multiplexed.

The subsystems of the CPRI link are **CPRI framer** and **CPRI deframer**. From the [11], the functions of each subsystems are shown in Table 2.2. The CPRI framer is responsible for RRH control and management, backhaul transport, media access control (MAC) layer, channel coding, add and remove cyclic prefix (CP) and MIMO processing. By contrast, the functions of channel filtering, ADC, DAC, upconverter, downconverter, carrier multiplexing, power amplifier and low noise amplifier are implemented by CPRI deframer.

Table 2.2. CPRI functions

Functions of CPRI framer		Functions of CPRI deframer	
Downlink	**Uplink**	**Downlink**	**Uplink**
RRH control & management		Add CP (optional)	
Backhaul transport		Channel Filtering	
MAC layer		D/A conversion	A/D conversion
Channel Coding Interleaving Modulation	Channel De-coding Interleaving Demodulation	Up conversion	Down conversion
Add CP	Remove CP	Carrier Multiplexing	Carrier De-multiplexing
MIMO processing		Power Amplifier	Low Noise Amplification

2.2. Power Amplifier (PA)

In this thesis, we assume that the loss from the fiber-optic link is occurred because of the long distance transmission. To compensate for the power loss generated from the fiber optic, a power amplifier (PA) need to be attached after the fiber-optic link. The PA is an electronic device that converts the low power RF signal to the high power signal. The PA achieves the power amplification by multiplying the input RF signal with a gain factor that results in the amplified signal which has a higher signal level compared with the original signal.

Depending on the input power, the PA is regarded as linear if the input power is within the range of linear amplification. In case that input power is operated outside of the linear range or within the saturation region of its characteristics, the PA will be recognized as a nonlinear amplifier. In order to achieve the maximum efficiency, the input power is usually decided to operate the PA near its saturation point. However, when the input power has varied amplitude, the nonlinear distortion such as intermodulation distortion (IMD) will occur to the output signal which degrades the system performance.

There are many ways to model the nonlinear characteristics of PA. The researchers proposed to use two types of model which are with memory and memoryless. The memoryless PA achieves a linearization performance, while the memory can model the system more accurately [12]. The following three subsections (2.2.1, 2.2.2, 2.2.3) describe the fundamental memoryless model that will be represented only AM/AM and AM/PM conversion. Then, the following two subsections (2.2.4, 2.2.5) shows the way to determine the PA quality and nonlinearity.

2.2.1 Saleh Model

The Saleh model was originally proposed to model a Traveling-Wave Tube Amplifier (TWTA), which can be computed using the memoryless nonlinearity model, as referenced in [13]. The AM/AM conversion of an amplifier is represented by

$$A(|x|) = \frac{\alpha_a |x|}{1 + \beta_a |x|^2}. \tag{2.1}$$

Similarly, the AM/PM conversion is represented by

$$\Phi(|x|) = \frac{\alpha_\phi |x|^2}{1 + \beta_\phi |x|^2}, \tag{2.2}$$

where $|x|$ is the amplitude of the input signal. The α_a and β_a are coefficients to adjust the output amplitude, while the α_ϕ and β_ϕ are coefficients to adjust the output phase rotation.

As shown in the above equations, the AM/AM and AM/PM conversions are based on the coefficients and varied amplitude of the input signal. To desire the appropriated parameters, the output and input signals can be measured to find the relationship, which depends on an application of the PA.

2.2.2 Ghorbani Model

The Ghorbani model was created to represent the Solid State Power Amplifier (SSPA) nonlinearity. This model uses eight parameters to fit the equations which are a_1, a_2, a_3, a_4 and $\phi_1, \phi_2, \phi_3, \phi_4$ for AM/AM and AM/PM conversion, respectively. The AM/AM conversion is represented by

$$A(|x|) = \frac{a_1 |x|^{a_2}}{1 + a_3 |x|^{a_2}} + a_4 |x| . \tag{2.3}$$

Similarly, the AM/PM conversion is represented by

$$\Phi(|x|) = \frac{\phi_1 |x|^{\phi_2}}{1 + \phi_3 |x|^{\phi_2}} + \phi_4 |x| . \tag{2.4}$$

As shown in the equations, the Ghorbani model can provide a higher nonlinear characteristics compared with Saleh model. However, these parameters can be configured to get the same nonlinear results with Saleh model.

2.2.3 Rapp Model

Rapp model was proposed to model the SSPA nonlinearity. However, this model simplified the equation by calculating only AM/AM conversion, because the phase distortion is negligibly small compared with TWTA. The AM/AM conversion can be represented by

$$A(|x|) = v \frac{|x|}{\left(1 + \left[\frac{v|x|}{|x|_0}\right]^{2p}\right)^{\frac{1}{2p}}}, p > 0, |x|_0 \geq 0, v \geq 0, \tag{2.5}$$

where p is a smoothness factor, $|x|_0$ is the output saturation level and v is a small signal gain.

In order to determine the PA quality and nonlinearity, there are two main keys which are the 1-dB compression (P1dB) and the third-order intercept point (IP3). The details of these measurements are shown in the following subsection.

2.2.4 1-dB Compression

Due to the fact that, all of the PA has their specific linear range. Fig. 2.8 shows the relationship between the input and output power. When the input power increases, the output power is also increased as well. However, at some point, the output begins to reduce the increasing rate until reaching the saturation point. This curve results in nonlinearity which creates the signal distortion.

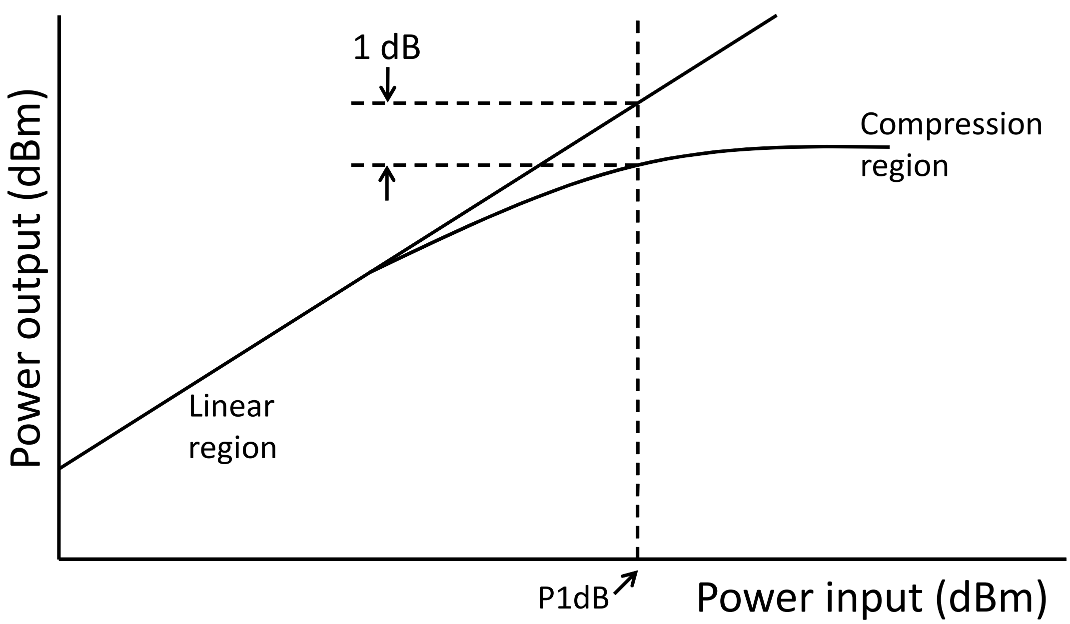

Figure 2.8. 1-dB compression

It is important to know the beginning of saturation point, P1dB point, which is defined by the different of 1 dB drop between the linear line and nonlinear line. From this information, we can adjust the input power in order to prevent the nonlinear distortion.

2.2.5 Third-order Intercept Point

When the single tone signal passed through the nonlinear devices, the harmonic distortion will occur at far from the desired signal. However, this problem can be neglected by properly design the filter. In the case of two or more signals are passed through the nonlinear amplifier, the IMD will occur in the system. Assuming that these designed signals are close together, the IMD, such as third-order and fifth-order, will produce in the range of amplifier bandwidth, which IMD can interfere with the desired one.

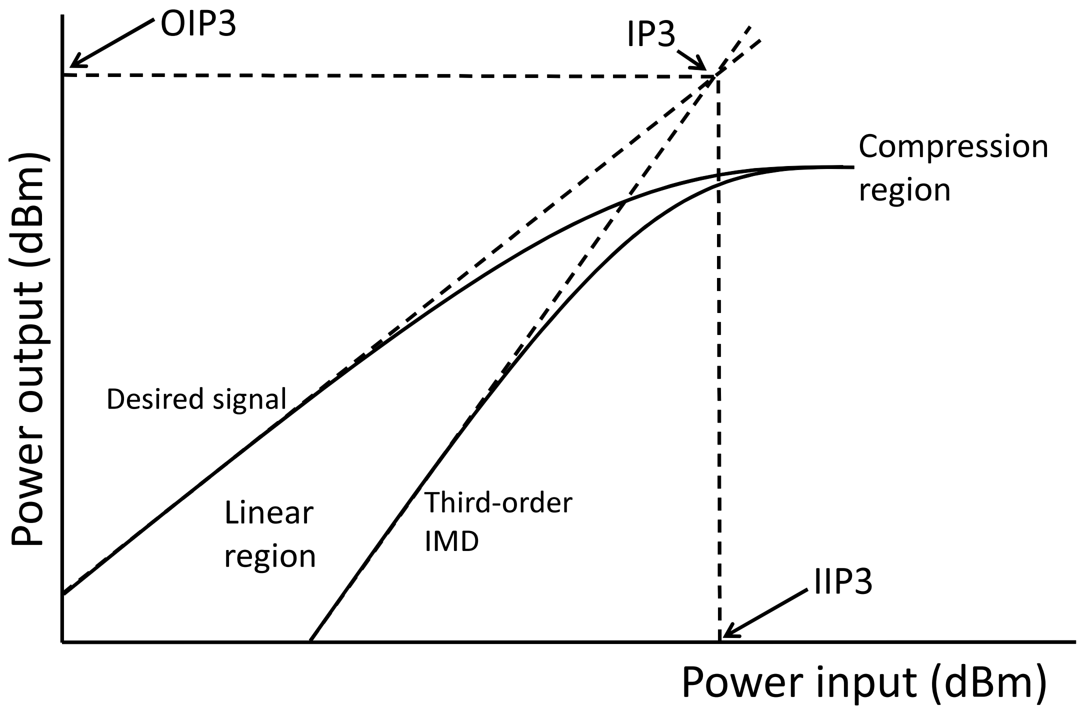

Figure 2.9. Third-order intercept point

The third-order IMD is the strongest distortion with the increasing rate about three times of the first-order. This ratio is calculated by converting the signal power to the logarithm scale. From Fig. 2.9, the IP3 can be observed by extending the linear portions; then these signals will intercept at the IP3 point. The higher output third-order intercept point (OIP3) means the better nonlinearity of the PA, and lower IMD.

2.3. Centralized Radio Access Network (C-RAN) Architecture

Nowadays, the most of wireless Internet access comes from the indoor location. Data communication traffic at the indoor location is significantly increased because the smart devices equipped with different kinds of wireless modules such as the 3-rd generation cellular (3G), LTE and Wireless Fidelity (WiFi). As for the mobile backhaul and fronthaul, mobile backhaul referred as distributed radio access network (D-RAN) is based on the point-to-point link. The baseband processing unit (BBU) attached one-by-one with the RRH through the CPRI [14]. To deploy the LTE cells in indoor place, the number of BBUs increases as well as increasing the number of RRHs.

The C-RAN has been employed to support the coordinated multi-point (CoMP), enhanced inter-cell interference coordination (eICIC) and carrier aggregation (CA). The main purpose of the C-RAN is to separate the BBU from the RRH and merge the function of BBU into the CCS. While, in the D-RAN, all of the components are installed in only one area. The configuration of RRH can be simplified by introducing the RoF link. The C-RAN can be categorized into two configurations: digitized RoF and analog RoF. We noted that the RRH and RAU are

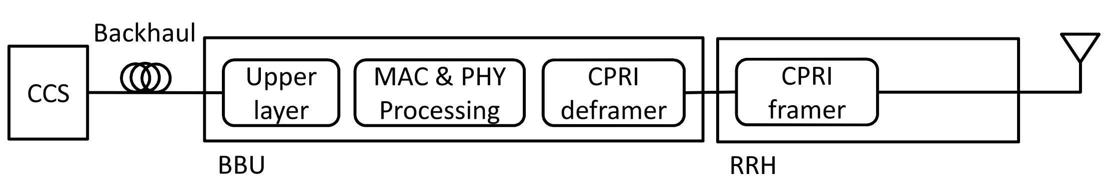

Figure 2.10. D-RAN

implemented in the digitized RoF and analog RoF, respectively. The variety of architecture mentioned above are shown in Fig. 2.10, Fig. 2.11 and Fig. 2.12. In the case of using digitized RoF, the CPRI with the point-to-point connection is employed as a fronthaul link. In this architecture, the common MAC and physical (PHY) layers can manage radio resource for plural RRHs. There is no degradation due to intermodulation distortion in CPRI link compared to analog

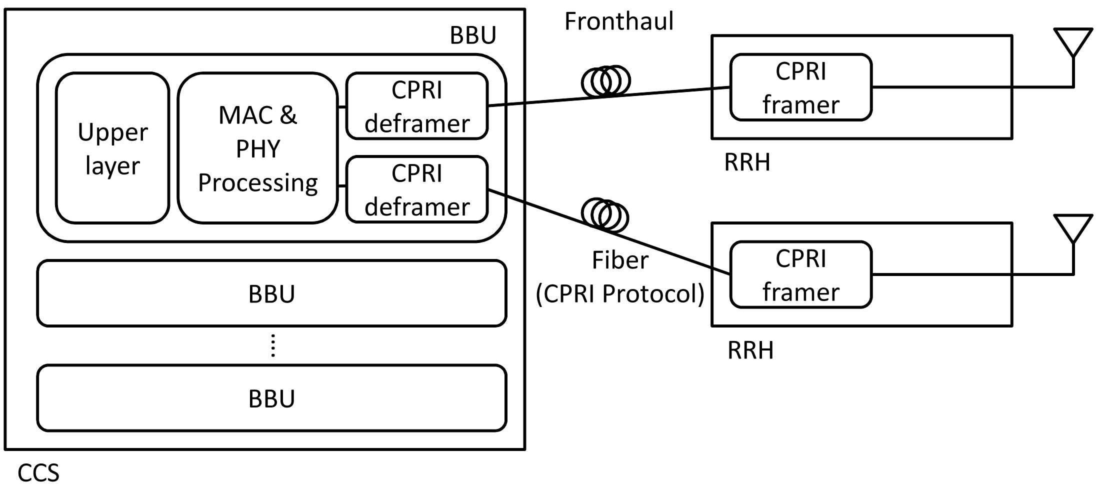

Figure 2.11. Digitized C-RAN

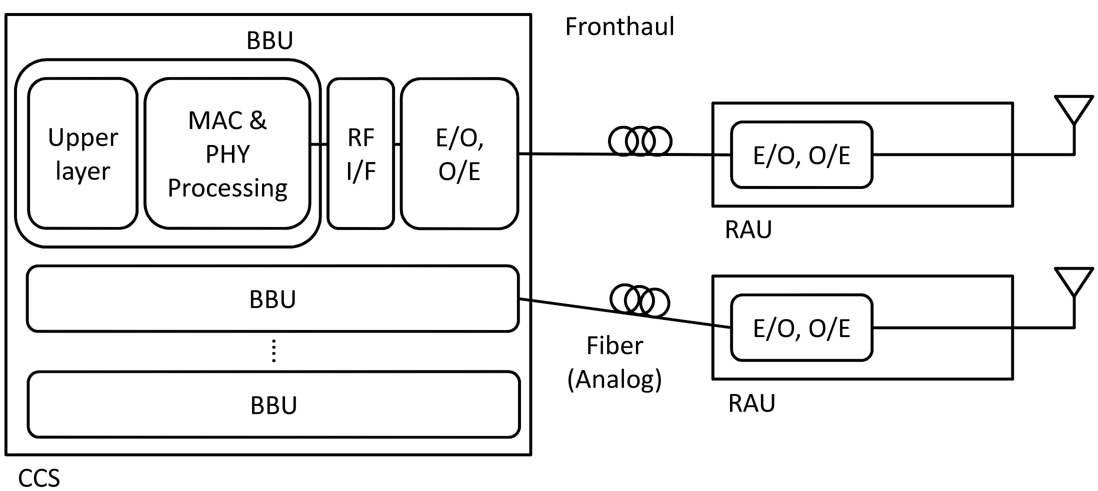

Figure 2.12. Analog C-RAN

RoF. However, digitized RoF requires a large amount of bandwidth to transport RF signal, and many processes need to be installed such as CPRI equipment and additional protocols [15]. In order to make the RAU simple and to support the next generation of the communication system as we discussed in this chapter, in all of the parts of this thesis, we propose to use the analog RoF with the C-RAN configuration as shown in Fig. 2.12. Moreover, by dividing BBUs from the RAUs and defining mobile fronthaul interfaces has many valuable advantages as given below.

1. **Cost reduction** by the service providers can be classified as capital expenditures (CAPEX) and operating expenses (OPEX). CAPEX is the cost that generated by deploying infrastructure and implementing network interfaces equipment. While, OPEX results from the operational costs that the service provider pays to run the basic infrastructure, including energy bills, update costs and repairing. By installing a few BBUs in the CCS instead of implementing for every RAU can considerably reduce the installation times and network equipment costs.

2. **Energy saving** of the C-RAN is the criteria for service providers because it has a high impact on OPEX. As already mentioned by the cost reduction, the BBU centralization into the pool allows sharing some ecosystem such as air conditioning, power supplying and monitoring servers, thus taking advantage of some economies of scale.

3. **Resource sharing** is the main advantage that we use in Chapter 3. The overview of resource sharing in C-RAN has been investigated in [16], which is the spectrum sharing. Spectrum sharing may be performed by different kinds of allocation units such as channels used on the Wi-Fi and the resource blocks from LTE frames. Moreover, the unused resources can be shared through dynamic spectrum access using the benefits of BBU pools.

In the ways that are easy to understand, we summarized the difference between D-RAN, C-RAN with digitized RoF, and C-RAN with analog RoF. The one important thing is that the C-RAN with analog RoF can avoid the handover process even the mobile users move across the cell as shown in Table 2.3. According to these advantages, we propose the algorithm for control the BBU and RAU

Table 2.3. D-RAN and C-RAN summarization

	RoF link bandwidth utilization	Nonlinearity	Handover reduction	BBU reduction	CA, CoMP, eICIC
D-RAN	Low	Low	No	No	No
C-RAN (Digitized RoF)	Low	Low	No	Yes	Yes
C-RAN (Analog RoF)	High	High	Yes	Yes	Yes

combinations in Chapter 3. However, the nonlinear characteristic occurs when the analog RoF is employed. In Chapter 4, we propose two methods to alleviate the problem of IMD that is generated from nonlinearity of the system.

Chapter 3

Handover Reduction using Optical Matrix Switch for Indoor LTE Cell Deployment

According to [17], 80% of wireless data traffic originates from indoor locations. Mobile operators deploy the indoor equipment in order to build the radio access coverage. Mobile backhaul link for constructing small cell of the Long-Term Evolution (LTE) is composed of the baseband unit (BBU) and remote radio head (RRH), and these are connected by the optical link interfaces such as the common public radio interface (CPRI) or 10 Gbps Ethernet. These optical links can contribute to deploy LTE cell at the indoor location.

A problem in the deploying cell at the indoor location is that the cell size must be smaller than outdoor location, because of the limited transmitting power of the indoor equipment. Since the CPRI and Ethernet link is based on the point-to-point link, it is anticipated that the handover process between cells often occurs, that is, the processing data stream in a BBU is required to switch to the other one whenever a mobile user moves across beyond the currently connected cell. In order to reduce the handover, the [18] configures the mobility-prediction, which the positioning technique is additionally required for tracking the current position of the mobile user. This research proposes the other approach using the analog Radio over Fiber (RoF) transmission and the optical matrix switch. Fig. 3.1 shows the proposed configuration. Assuming that the LTE radio frequency (RF) transceivers are located in centralized control station (CCS), and the RF LTE signal is obtained from RF interface (I/F). The RF signal is transmitted between LTE transceiver and remote antenna unit (RAU) via the optical fiber link. At the RAU, the RF to optical (R/O) and the optical to RF (O/R) interfaces convert between the optical to the RF domain. This research assumes the intensity modulation-direct detection (IM/DD) as an optical I/F. Since the waveform format is analog, one optical stream can be easily distributed to multiple remote cells by dividing it passively. Therefore, RF resources of the bandwidth are shared among multiple cells using the optical matrix switch. The role of controller unit is to collect the resource usage of each BBU, then decides combination in the switch.

In the proposal, a cell where a large number of mobile users exist is combined with several neighboring cells. Therefore, the handover is no longer required at combined cell even though the mobile user moves out of the cell. The primary goal of the proposal is to reduce the number of handover compared to the point-to-point based network. As the secondary advantage of the radio resource sharing among cells, the required number of LTE transceiver equipment in the CCS can be reduced. In the previous papers [19, 20], the resource management has been modeled as an optimization problem that aims to minimize the number of BBUs, which is called as the heuristic bin-packing problem. However, the goal of algorithm limited to minimize the number of BBUs, while the number of handover is still high. In proposal, the neighboring cells are combined to one cell. Hence,

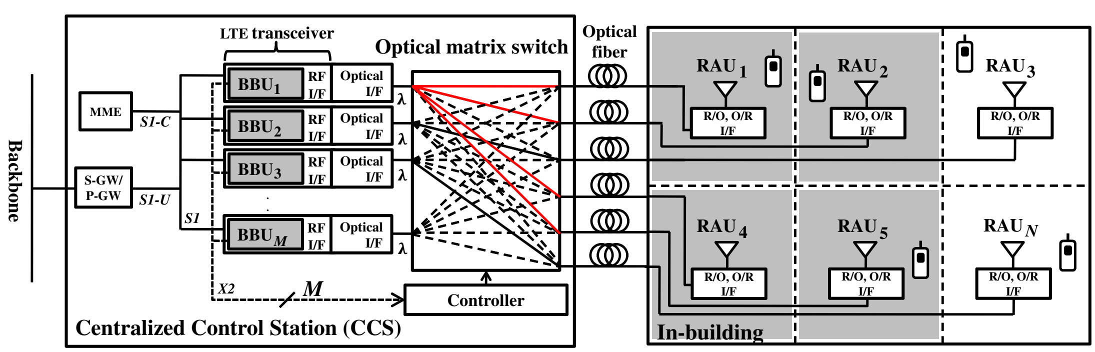

Figure 3.1. Analog C-RAN with optical matrix switch configuration

the resource sharing is able to reduce the BBU equipment accompany with the decreasing of the handover process. The number of BBUs, M, could be less than the number of RAUs, N.

3.1. Handover Procedure

Each BBU connects with the controller via $X2$ interface as shown in Fig. 3.1. The network components in the CCS are connected by the $S1$ interface, including the mobility management entity (MME), the serving gateway (S-GW), the packet data unit gateway (P-GW) and the BBUs. The $S1$-C and $S1$-U are the interface for control plane (C-plane) and user plane (U-plane), respectively [21]. These components and connections except controller are identical to the regular LTE system. In the regular LTE for configuring small cells, the C-plane and U-plane run over the macro cell and small cell fronthaul network separately. The MME manages the handover process. In our proposal, the MME operates handover process in the CCS through the $X2$ and $S1$-C interfaces. And the fronthaul elements including RAUs and fiber optics simply transfer the radio signal [22]. Therefore, the conventional handover process [23] can be introduced to our proposal without any modification in the protocol of $X2$ and $S1$-C interfaces.

In the proposal, the physical cell identity (PCI) is employed to identify the BBU like regular LTE system. Multiple RAUs share one PCI when multiple cells configure to the combined one. For example, in Fig. 3.1, radio signal transmitted from RAU of $1^{st}, 2^{nd}, 4^{th}$ and 5^{th} have the identical PCI when these RAUs share resource of BBU_1. The handover process is activated when the mobile terminal receives LTE signal with more than one PCI. At the beginning of the process, the source BBU sends a request to alternative BBU, and alternative BBU replies acknowledgment through the $X2$ interface. Then, the alternative BBU sends the request to the MME via $S1$-C interface in order to create a new session. Details of the procedure are shown in [23]. After the mobile terminal connects to the BBU, the mobile terminal will send the user data to the S-GW and P-GW through $S1$-U interface.

The handover procedure can be categorized in two cases [24]. The first case occurred when the users are moving across two RAUs which these RAUs must be served with different BBUs as shown in Fig. 3.2. In the cellular network, the handover from the users occurs as a majority, depending on the mobility movement. The second type of handover occurred when the optical matrix switch changes the connection as shown in Fig. 3.3. Even the users are not moving; the proposal periodically needs to be activated. The reason behind this is because the users have to re-establish the connection from serving BBU to another BBU. Since the controller requires the information on user density and user's offered load, the proposal is activated. This research evaluates the number of total handover for above two cases.

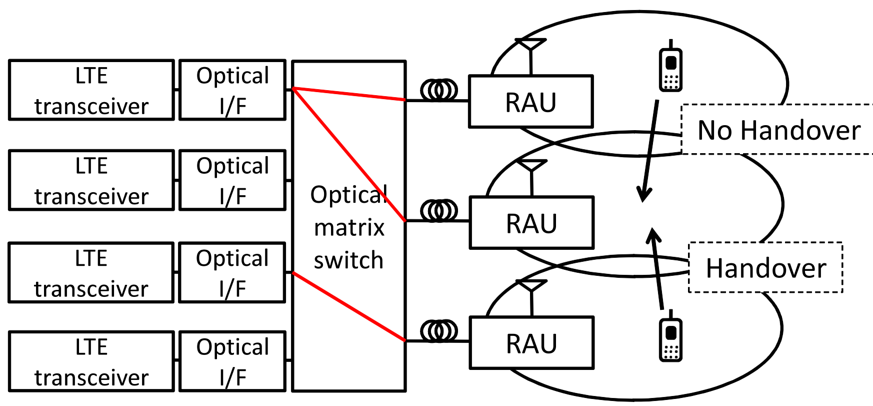

Figure 3.2. Handover driven by user mobility

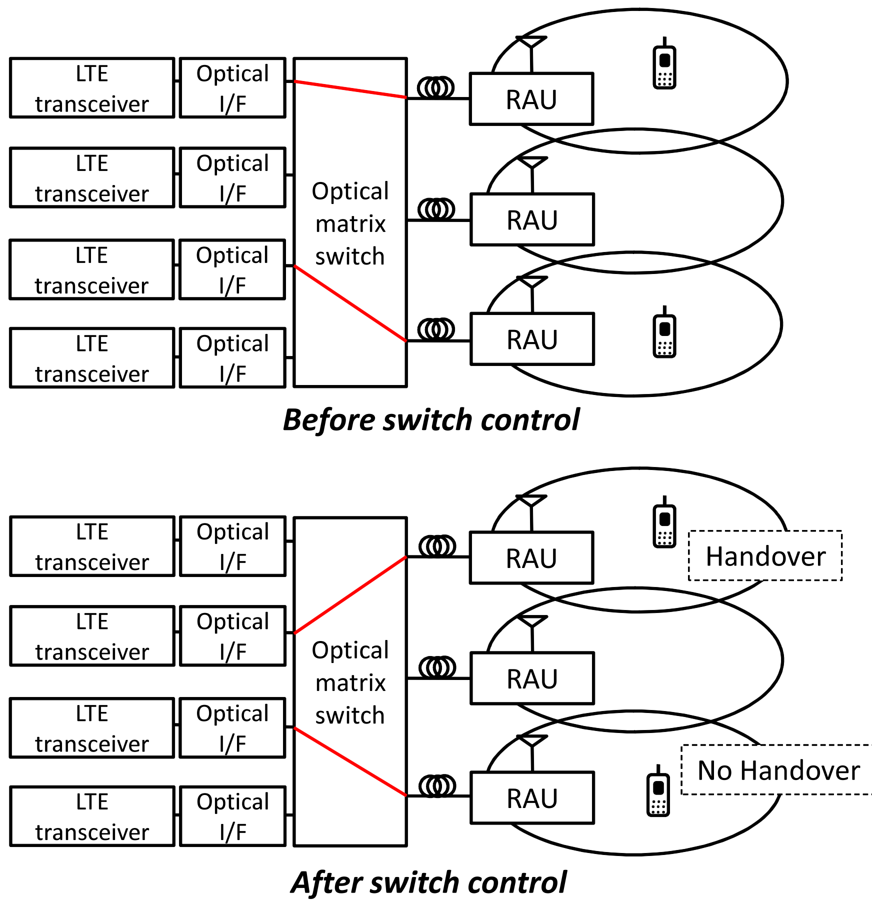

Figure 3.3. Handover for control

3.2. Proposed Algorithm for Controlling Optical Matrix Switch

In this research, the algorithm that minimized the number of handover by changing the topology of optical matrix switch is proposed. The algorithm gathers the neighboring RAUs to the same BBU, while satisfying the user demand. Since this algorithm based on the graph, the RAU and the connection between the adjacent RAUs are represented as vector and edge, respectively. In order to traverse the graph, breadth-first search (BFS) was deployed in the algorithm until the capacity of the BBU is full usage. We noted that all steps of an algorithm performed by the controller unit.

Fig. 3.4 shows the flowchart. At first, the optical matrix switch configures point-to-point link connection between BBU and RAU. We assumed that the controller has adjacency relationship for all RAUs. Let $G = (V, E)$ be a graph with N vertices; each vertex represents RAU in the system. The neighborhood of the vertex in graph G is connected by the edge, and the weight of all edges is the same. Two functions are defined as follows, nou$[n]$ gets the number of users connected to vertex n and eol$[n]$ gets estimated offered load on vertex n, $n = 1, \ldots, N$ and $|V| = N$. The controller can carry out nou$[n]$ and eol$[n]$ through the $X2$ interface. Set B_m is the combination set of RAU that will connect to one BBU of m-th, $m = 1, \ldots, M$. And set R is M set of B, then $R = \{B_1, B_2, \ldots, B_M\}$, for example, B_1 means the set of RAUs that connected to BBU of 1-st.

Algorithm 1 shows pseudocode. Our proposal is based on the BFS. The parameters are graph G and source, source is a vertex n with maximum nou$[n]$. In *line* $2^{nd} - 14^{th}$, the source vertex and its neighbor vertices are grouped in set B. Then, the elements in B will be assigned to one BBU. Above procedure repeats until the BBU is full usage. Then, the algorithm adds the set B to R as shown in *line* 21^{th}. In the last process, the algorithm returns set R.

After updating connection combination of optical matrix switch, resource usage is periodically monitored. Another BBU is activated when the estimated usage of BBU exceeds capacity, then switch the data stream to the BBU. In contrast, BBU with small usage is deactivated after switching its data stream to another BBU. Hence above monitoring process reduces the required number of LTE transceiver in the CCS.

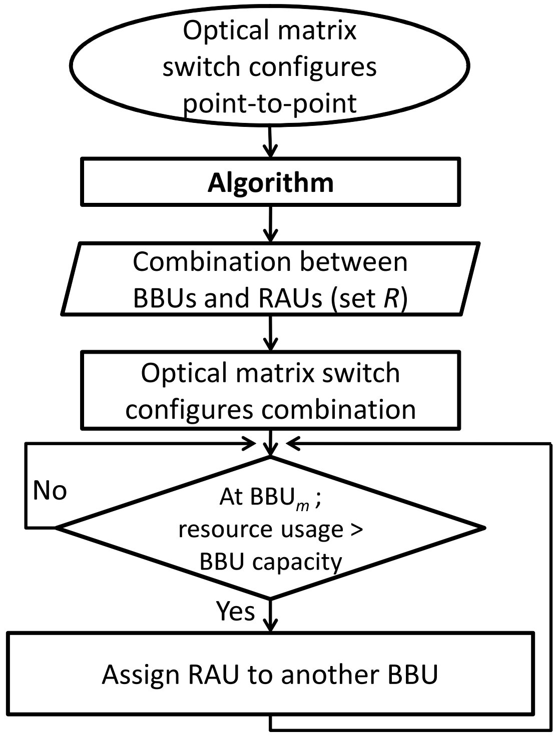

Figure 3.4. Flowchart

Algorithm 1 Proposed algorithm for controlling optical matrix switch

```
function COMBINATION(G, source)
    create empty queue Q and empty set B
    t_sum = 0
    t_sum = t_sum + eol[source]
    add source to B
    mark source in V
    Q.enqueue(source)
    while Q is not empty do
        u = Q.dequeue()
        for each unmarked vertex v that is adjacent to u do
            Q.enqueue(v)
            if t_sum + eol[v] ≤ BBU capacity then
                t_sum = t_sum + eol[v]
                add v to B
                mark v in V
                if all vertices in G is marked then
                    R ← R ∪ B
                    return R
                end if
            else
                R ← R ∪ B
                w ← unmarked vertex n with maximum nou[n]
                COMBINATION(G, w)
            end if
        end for
    end while
end function
```

3.3. Network Simulation

In this section, we compare our proposed algorithm with the bin-packing algorithm and the conventional point-to-point system using the centralized radio access network (C-RAN) configuration. The network simulator version 3 (ns-3) [25] is introduced to simulate the packet data convergence protocol (PDCP), radio link control (RLC), media access control (MAC) and physical (PHY) layers of the LTE system.

The scenario for simulation is performed as shown in Fig. 3.5, which represented the subway corridor. The RAUs were constructed in a grid formation, with the space of 30 meters. The number of RAU was 18, which all them attached on the hall roof, employing the transmission power of 10 dBm with the center frequency of 1.93 GHz. As an initial step, all of the mobiles were uniform randomly placed on the field before running a simulation. Two models for the simulating behavior of mobile user were employed: one-way constant walk mobility model [26] and random walk two-dimensional mobility model [27]. Each mobile user randomly requested the data traffic of 4/12/20/40 Mbps with its distribution ratio of 0.5/0.3/0.1/0.1, respectively. These users movement represents for the pedestrian. The other simulation parameters are shown in Table 3.1.

Table 3.1. Simulation parameters in the network simulation

Parameters	Value
Propagation loss model	Friis free-space model [28]
Handover algorithm	A3Rsrp [29]
Hysteresis of A3Rsrp	3.0 dB
Time to trigger of A3Rsrp	256 ms
Capacity for each BBU	200 Mbps
Simulation time	60 s
Speed of user	1, 2 m/s

It is anticipated that strong fading in radio channels must be generated at the overlapped area when the multiple cells are combined into one cell by the optical matrix switch. This kind of artificial fading occurs in both uplink and downlink radio channel. In our assumption, fading can be compensated by the channel equalization technique equipped in LTE system such as frequency domain equalization (FDE) [30]. The performance evaluation assumes that fading has a negligible impact on the process of handover and also the number of handover.

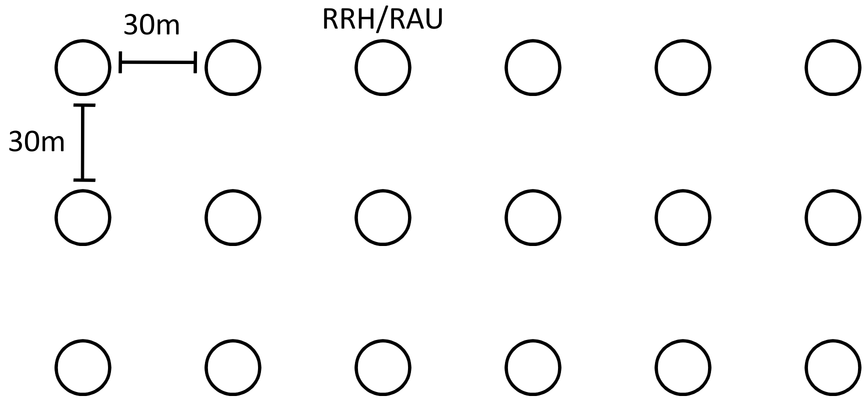

Figure 3.5. Layout of network simulation (plane figure)

Fig. 3.6 shows the results when the average number of users per RAU is increased. In the case of user's speed is 1 m/s, we can see that the number of handover decreased about 13.43 % compared with point-to-point configuration. However, when the mobility speed increases, more effectiveness of our proposal can be achieved because of the handover from users movement considerably increased. When the user's speed is 2 m/s, the number of handover reduced about 38.27 % compared with point-to-point configuration. From this reason, we can conclude that the C-RAN with our configuration will result in high effect in terms of the handover reduction when the number of handover from users movement is high.

Fig. 3.7 shows the number of handover comparison between the user's movement and the switch configuration. When employing point-to-point, the handover from users is extremely high compared with the handover from switch configuration. Here, the handover from the switch is no longer activated since the configuration is point-to-point. However, when using our proposal, the number of handover from users is drastically decreased. Moreover, in the case of only one user attached to each RAU, there is no handover process occurred from users since all of the RAU is connected to only one BBU as shown in Fig. 3.9.

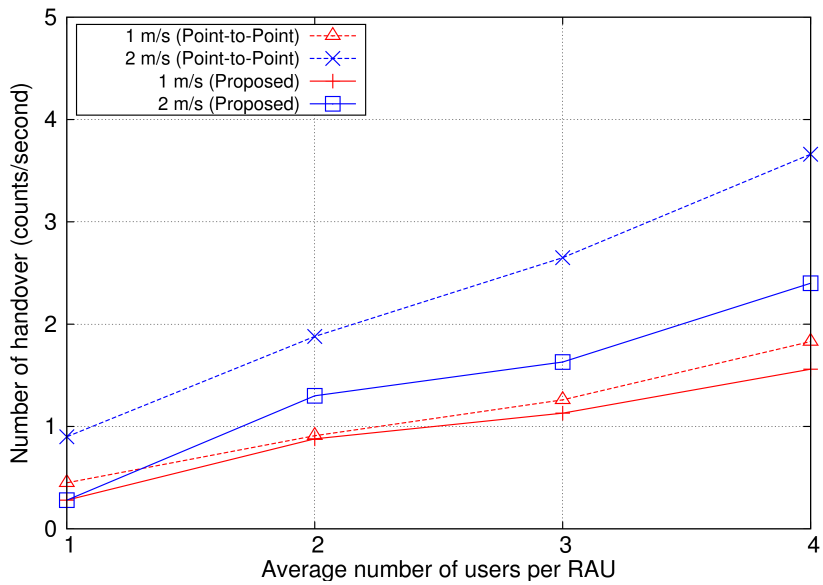

Figure 3.6. The number of handover when the user's speed is changed (One way constant walk)

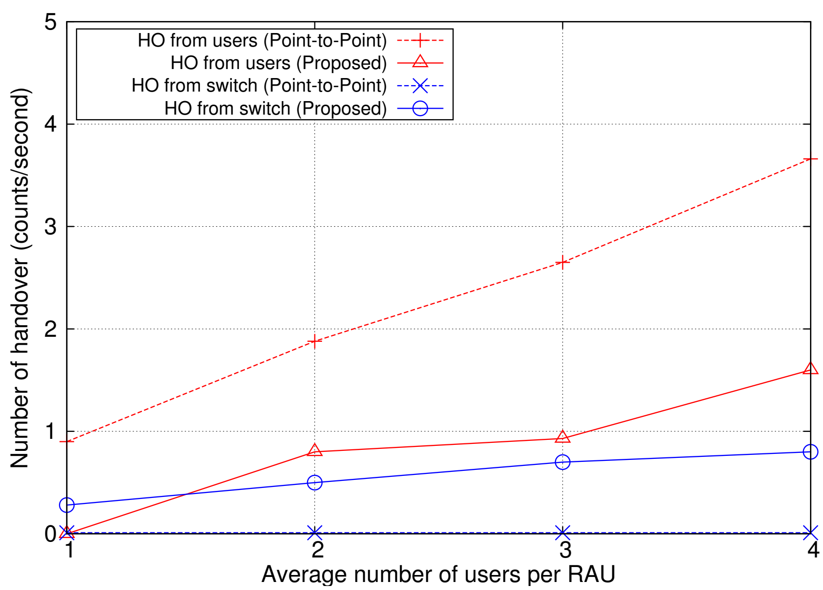

Figure 3.7. Comparison between the handover from users and switch configuration (One way constant walk, user's speed = 2 m/s)

Fig. 3.8 and Fig. 3.9 show the performance comparison when the mobility model is one-way constant. The proposal can reduce the number of handover by 38.27% compared with the point-to-point based network. Besides, the number of BBUs is a bit higher than the bin-packing algorithm. In this figure, all of RAUs are connected to one BBU in both of proposal and bin-packing in the case of the average number of user is 1. The handover process driven by user mobility were not occurred. The number of handover of 0.28 occurred by only for control the switch configuration. Fig. 3.10 and Fig. 3.11 show the performance when the mobility model is random walking. The proposal can reduce the number of handover by 36.12% and 23.25% compared to point-to-point based network and bin-packing algorithm, respectively. It is found that there is a trade-off between the number of BBUs and the number of handover.

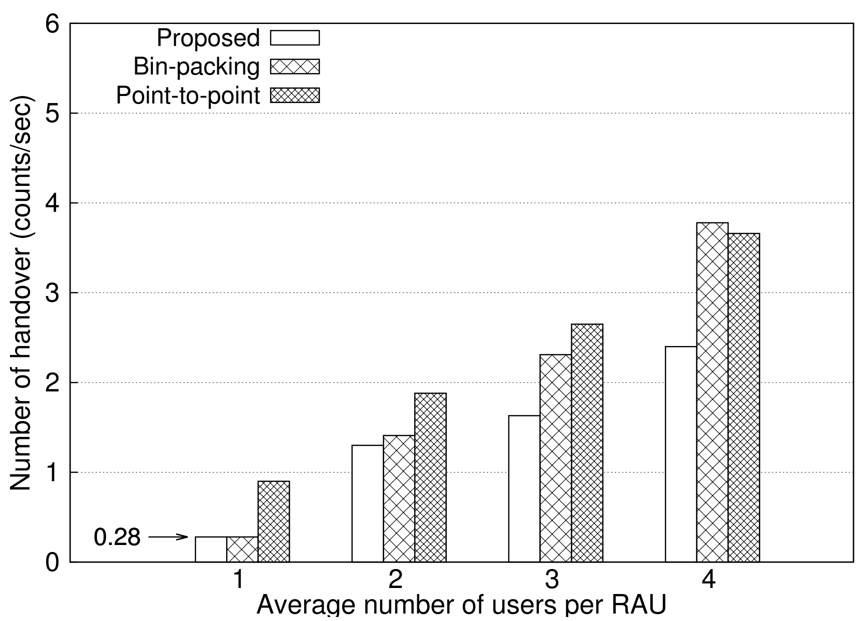

Figure 3.8. Number of handover (One way constant walk, user's speed = 2 m/s)

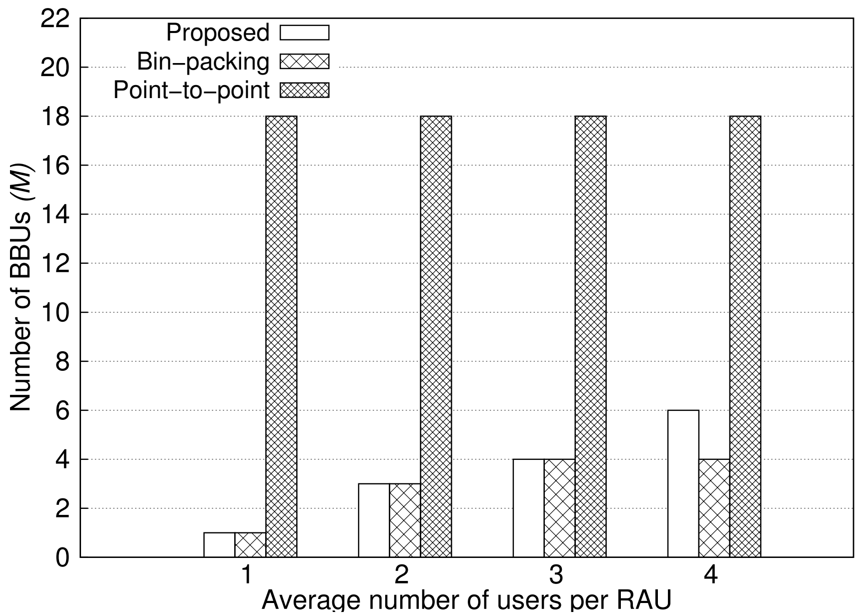

Figure 3.9. Number of BBUs (One way constant walk, user's speed = 2 m/s)

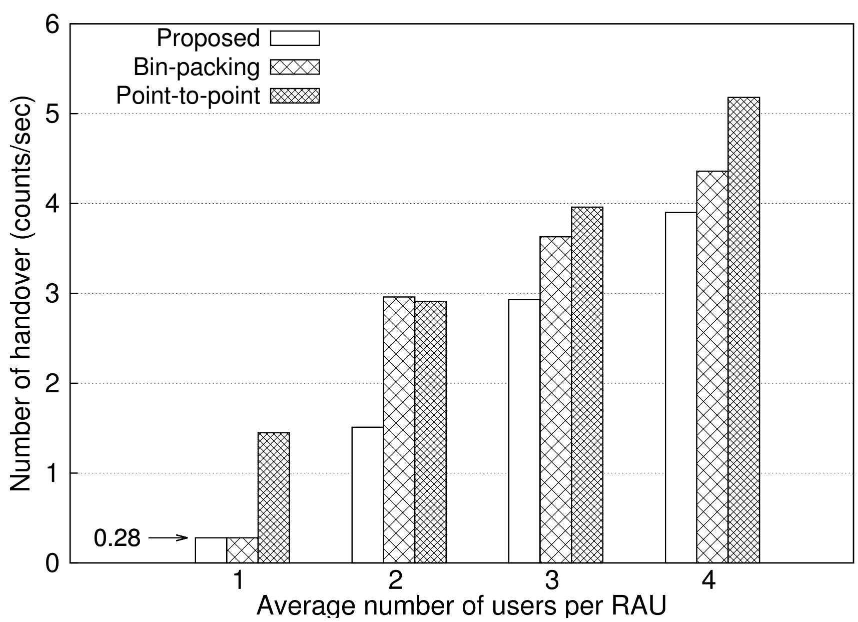

Figure 3.10. Number of handover (Random walk, user's speed = 2 m/s)

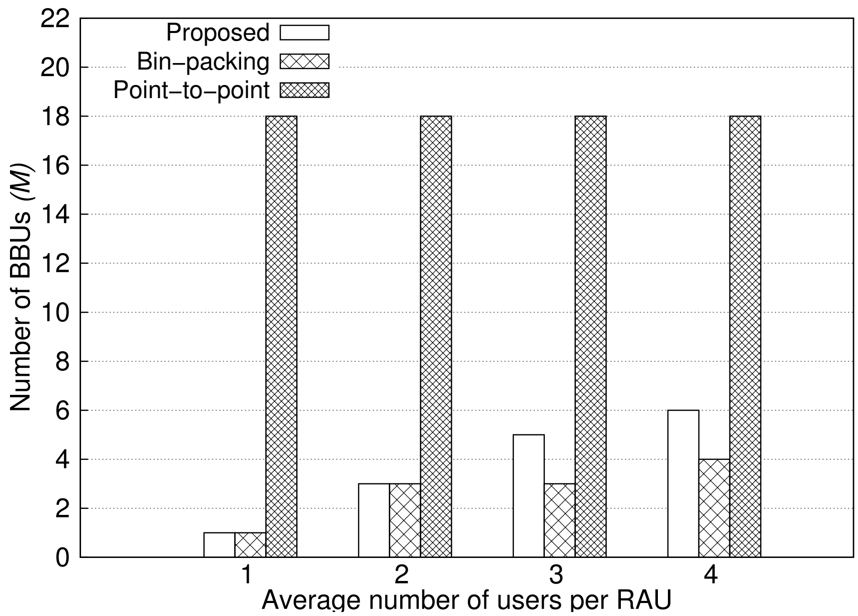

Figure 3.11. Number of BBUs (Random walk, user's speed = 2 m/s)

However, in the case of the high number of users per RAU, the effectiveness of our proposal will become small as shown in Fig. 3.12. The reason is that there are a lot of BBUs that were activated. Therefore, the combined cell will spread to the small cell, and turn the connection into the point-to-point as shown in Fig. 3.13. From these results, when the average number of users per RAU is more than 12, our proposal configures the point-to-point connection as the number of BBUs is increased to 18, and its performance is equal to the conventional point-to-point.

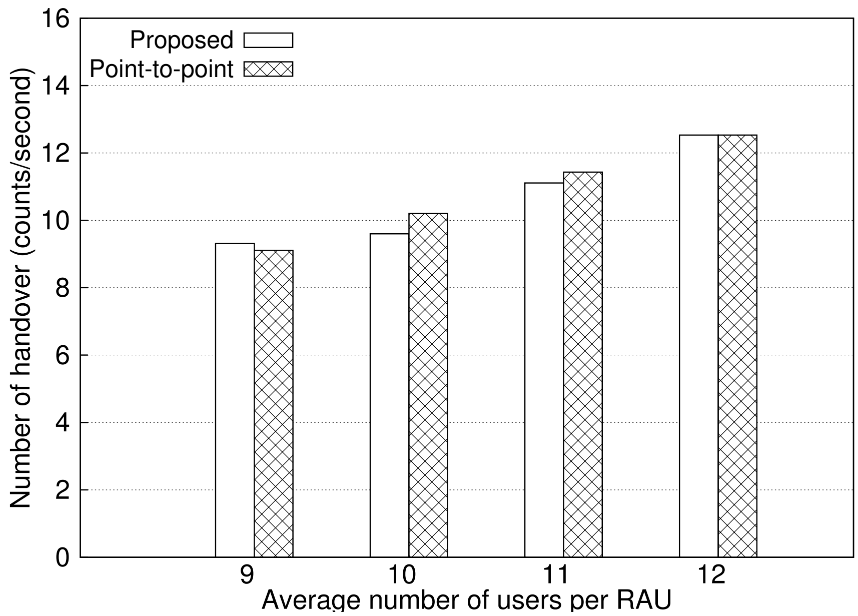

Figure 3.12. Number of handover (Random walk, user's speed = 2 m/s)

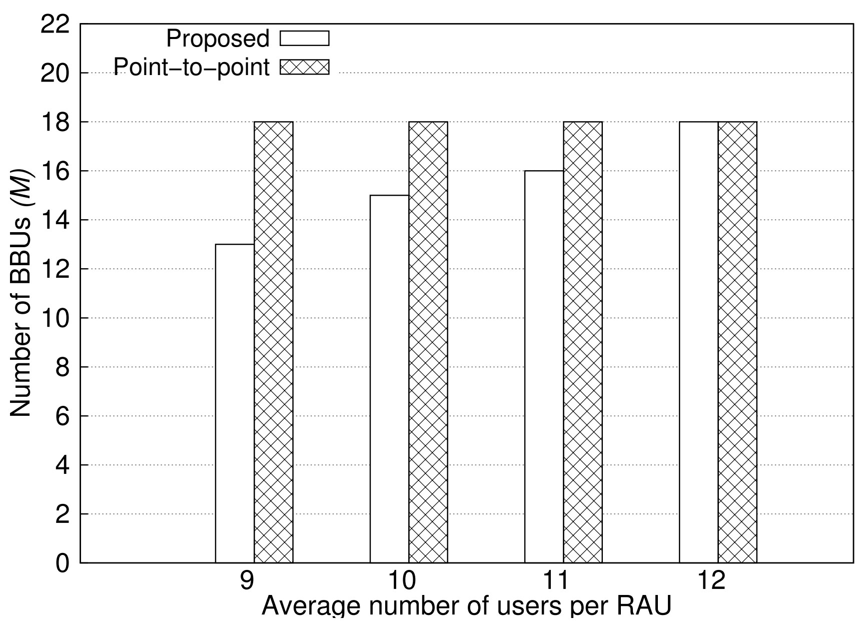

Figure 3.13. Number of BBUs (Random walk, user's speed = 2 m/s)

3.4. Conclusion

In this research, we have introduced a new mobile fronthaul configuration using the optical matrix switch for the LTE cell deployment at the indoor location. The proposal combines the several neighboring RAUs into a single BBU in order to reduce handover. From the results, our proposal drastically decreases the number of handover accompany with the number of BBUs equipment. Our proposal can reduce the number of handover by 38.27% and 36.12% compared with the point-to-point based network when the mobility models are one-way constant and random walking, respectively. Moreover, in the cases of high-speed users, the handover reduction of our proposal can be further improved.

Chapter 4

Quality-based Channel Allocation Scheme with Predistortion in Multi-channel Radio over Fiber System

Analog Radio over Fiber (RoF) is low-volume of the fiber optics, used for the satellite communication and the cellular radio unit feeding. Moreover, the impairments and nonlinear responses of the analog equipment, such as distortion and noise, degrade the system performance. However, with the need of attentive manufacturing and high cost, the analog RoF is still required for the service providers. The reason behind this is because the flexibility and simplicity at the antenna site, whereas the function of remote antenna unit (RAU) is simplified by removing the analog to digital converter (ADC) and moving radio frequency (RF) frontend functions to the centralized control station (CCS). Several service providers are now competing in this way by implementing the application such as in-building distributed antenna systems. Fig. 4.1 shows an application using the RoF: the fiber-optic connects with the RAU and the CCS. At the RAU, an antenna is located for radiating the downlink radio signals and receiving the uplink radio signals.

The motivation of this study is that we want to reduce the intermodulation distortion (IMD) problem in uplink over the multi-channel analog RoF system.

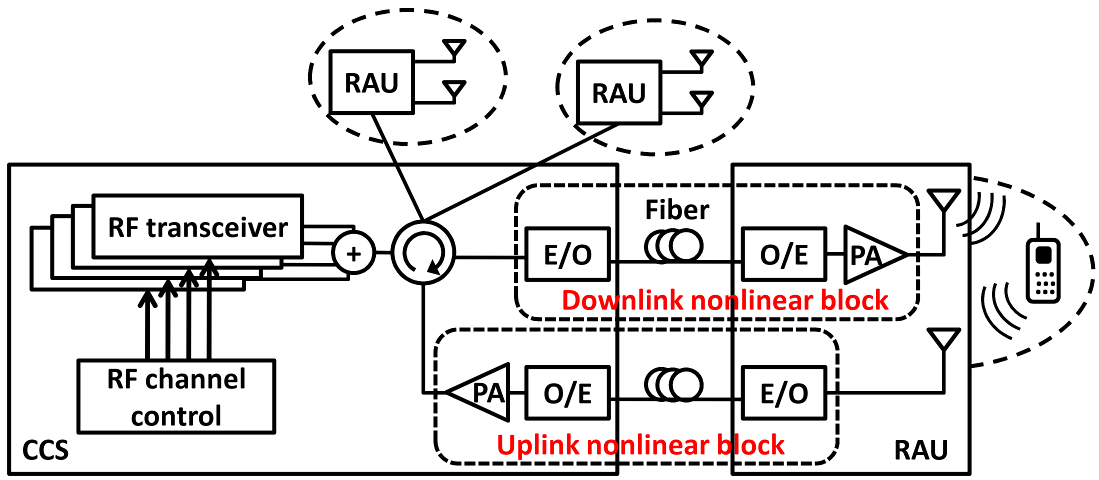

Figure 4.1. Application of RoF

We introduce two methods for nonlinear compensation: dynamic channel allocation (DCA) and predistortion (PD). To provide an accurate evaluation regarding the throughput performance, this research introduces a network simulation that can simulate the media access control and physical layers.

4.1. The IMD Problem in Uplink over Multi-channel RoF System

In this subsection, the uplink IMD problem due to the coupled downlink signal is investigated. Fig. 4.2 shows the uplink IMD problem in the multi-channel RoF system. We assume that the backbone is the IP-based network. Therefore, a network interface (I/F) is required between the backbone and the modulation devices. The backbone is connected to the network I/F, followed by the baseband modulator, upconverter, electrical to optical converter (E/O), fiber link, optical to electrical converter (O/E) and power amplifier (PA). In the downlink stream, two RF signals will modulate the optical carrier using the E/O. The IMD will appear at the output of the PA. After that, the RF signals and IMD are radiated from the transmitting antenna. In the uplink stream, the signal transmitted from the mobile station is forwarded to the CCS. Due to the coupling between the transmitting and the receiving antennas in the RAU, the IMD that was generated from the coupled downlink signals interferes with the uplink signal at the output of the PA in the CCS. This coupling could be alleviated using the antenna separation. For the antenna separation, we assume that the spacing between Tx/Rx antennas is shorter than the air propagation distance between the mobile station and the Rx antenna. If antenna directivity is omnidirectional, the power of the coupled RF signal is larger than the received uplink signal, which will result in a serious IMD interference at the CCS.

As for the antenna coupling, the radiating and the receiving antennas will be coupled together when placed close together at the RAU. Therefore, it is necessary to maintain the high isolation ratio or coupling loss (CL) between the two antennas. There are many methods to solve this problem, one being to introduce a circulator device that switches between the uplink and the downlink within one antenna. The isolation ratio of the ordinary circulator is about 15-20 dB [31], depending on the manufacturing process. The other two methods are the directive antenna [32] and the polarization duplex [33]. They are effective ways to increase the CL between the uplink and the downlink antennas. However, the numerical analysis in this research shows that the isolation ratio of 30 dB is not enough to obtain a sufficient number of available channels in the uplink when the number of active channels is more than 9. This analysis is described in subsection 4.3.1. In the case of low CL, the high level of the coupled downlink signal will interfere with the uplink antenna. However, when the CL is high, the coupled downlink signal is decreased, which reduces the level of IMD interference in the system. We evaluated the impact of the CL, as will be explained later in this research.

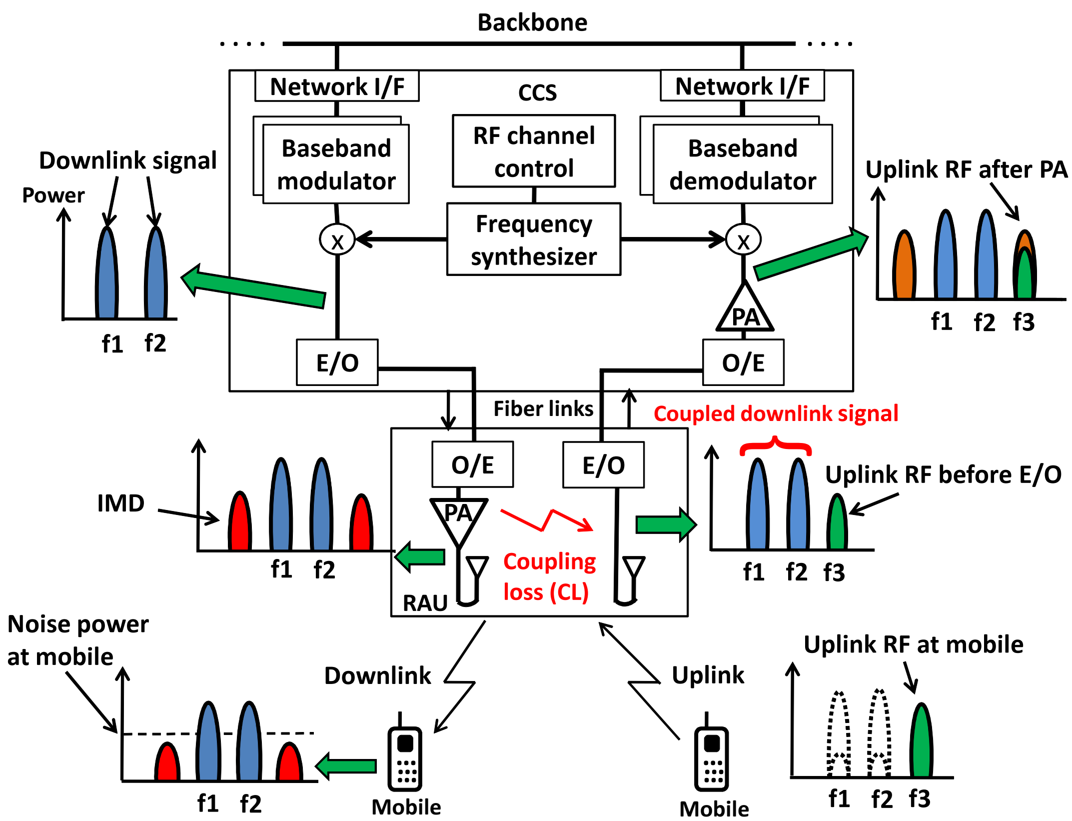

Figure 4.2. IMD between RF up/down link in multi-channel RoF

4.2. Loss and Gain from the RoF Components

In the telecommunication services, the fiber-optic link is an emerging technology to serve the increasing bandwidth demand. The main purpose of the fiber-optic link is to send the RF signal between the CCS and the RAU. Fig. 4.3 shows the three components of the fiber-optic link consisting of E/O, optical fiber, and O/E. In the E/O, the RF signal modulates the light source using the laser diode, and then transmits it over the fiber link. The fiber-optic is a stable medium with low loss. The loss can be around 0.4 dB/km at wavelength 1310 nm and 0.25 dB/km at wavelength 1550 nm [9]. At the O/E, the light is detected by the photodiode, which converts the light back to electrical current. This type of optical link is known as intensity modulated-direct detection (IM/DD).

Due to the power loss produced by the fiber link, a PA is required after the fiber-optic link block [34]. A PA is widely employed in communication systems. However, it is also a component that results in a more complicated nonlinearity characteristic [35]. The nonlinear from PA has a higher impact than the nonlinear from the fiber link. Therefore, we only utilize the nonlinear of the PA to model the nonlinear characteristic of the system [36].

The linearity of the system is extremely important for the RoF. In practice, all nonlinear responses of the optical modulators and amplifiers will generate impairments on the performance of the transmission system. The IMD usually utilizes the product order as a metric to show the level of distortion near the desired frequency bands, though. There are many different product orders such as the third and fifth orders, the third-order IMD having the largest impact on a single octave transmission system.

To introduce the IMD model from the PA after the optical fiber link, the general signal waveform used for the multi-carrier signal s as a function of time t is given as

$$s(t) = \sum_{m=1}^{M} A_m \cos(2\pi(f_c + f_m)t + \phi_m), \tag{4.1}$$

where f_c is the center frequency, $f_c + f_m$ is the RF carrier frequency of the m-th carrier, A_m is the amplitude of m-th carrier, ϕ_m is the initial phase and M is the number of active RF carriers. The real part of the complex signal can be written

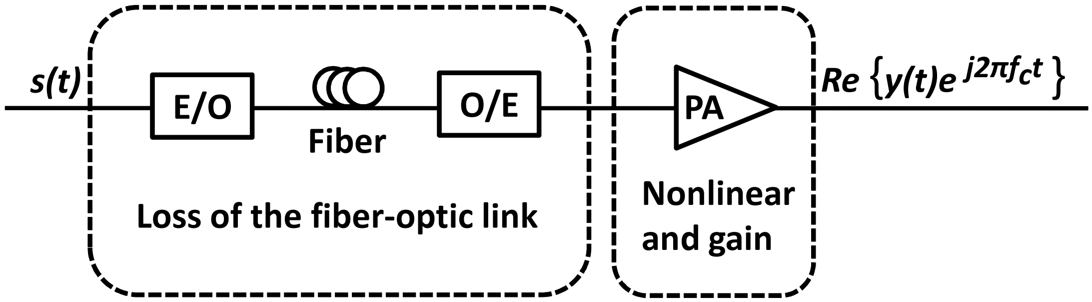

Figure 4.3. Nonlinear block

as

$$s(t) = Re\left\{e^{j2\pi f_c t} \cdot \sum_{m=1}^{M} A_m e^{j(2\pi f_m t + \phi_m)}\right\}, \tag{4.2}$$

where $x(t) = \sum_{m=1}^{M} A_m e^{j(2\pi f_m t+\phi_m)}$ is the equivalent low-pass expression of the signal.

To model the nonlinear characteristics, the nonlinear block can be represented in two parts as shown in Fig. 4.3. This will be explained in the following two subsections.

4.2.1 Loss of the fiber-optic link

The first block contains three main components: E/O, optical fiber and O/E. The link design consists of a connection between the laser diode output in E/O and the input of the photodiode in O/E.

According to [9], the RF loss (or gain) [dB] over the optical link (G_{LINK}) is a function of the laser diode efficiency (η_L), the fiber loss (L_O), the photodiode efficiency (η_P) and the ratio of the output to input impedances (R_{OUT}/R_{IN}), all of which can be represented by

$$G_{LINK}[\text{dB}] = 20\log(\eta_L \eta_P) - 2L_O + 10\log(R_{OUT}/R_{IN}). \tag{4.3}$$

The slope efficiency, which is the plot of the laser output power against the input power, is specially designed in this research. We assume that the η_L, η_P and L_O values are 0.25 W/A, 0.90 A/W and 1.5 dB, respectively. The R_{OUT} and R_{IN} impedances are 50 ω. When calculating the G_{LINK}[dB] using the aforementioned parameters, the result will be -16 dB; which will limit the applications of the optical fiber. To compensate for the power loss generated from the fiber link, a PA with a gain of 16 dB is required after the fiber-optic link block.

4.2.2 Nonlinear and gain of the PA

In this research, the nonlinear of the PA after the O/E can be represented using the Saleh nonlinear model. This model was originally proposed to model a stronger nonlinearity than the polynomial representation. It can also apply to any solid-state PA.

We use the RF impairments library of the MATLAB/SIMULINK [37] to calculate the spectrum of the output signal $y(t)$ after passing through the PA. The Saleh model can be computed using the memoryless nonlinearity model, as referenced in [13]. The input signal $x(t)$ is separated in terms of the magnitude and angle components. Then, AM/AM and AM/PM conversions are applied to the magnitude and the phase of the signal, respectively. Eventually, the last process will combine the new magnitude and angle components into a complex signal $y(t)$.

The AM/AM conversion of an amplifier is represented by

$$A(|x|) = \frac{\alpha_a |x|}{1 + \beta_a |x|^2}. \tag{4.4}$$

Similarly, the AM/PM conversion is represented by

$$\Phi(|x|) = \frac{\alpha_\phi |x|^2}{1 + \beta_\phi |x|^2}, \tag{4.5}$$

where $|x|$ is the amplitude of the input signal. The α_a and β_a are coefficients to adjust the output amplitude, while the α_ϕ and β_ϕ are coefficients to adjust the output phase rotation. To achieve the PA gain of 16 dB, the parameters $\alpha_a = 6.3122$, $\beta_a = 20.1517$, $\alpha_\phi = 90.0033$ and $\beta_\phi = 20.1040$ were used in the Saleh model.

We use the third-order intercept point (IP3) in order to analyze the quality of PA. The two-tone of RF signals passed to the PA as the input. Then, the output signal $y(t)$ is converted to the frequency spectrum using the fast Fourier transform (FFT). The power of the desired signal and IMD over the channel i (f_i) can be obtained. From Fig. 4.4, the input third-order intercept point (IIP3) and the output third-order intercept point (OIP3) are about +11 dBm and +27 dBm, respectively. In this research, we assume that the maximum transmission power is +16 dBm for the WiFi system. The signal power is alleviated by the fiber link loss of 16 dB. Therefore, the maximum input power to the PA nonlinear block is 0 dBm, which is lower than its saturation point in Fig. 4.4.

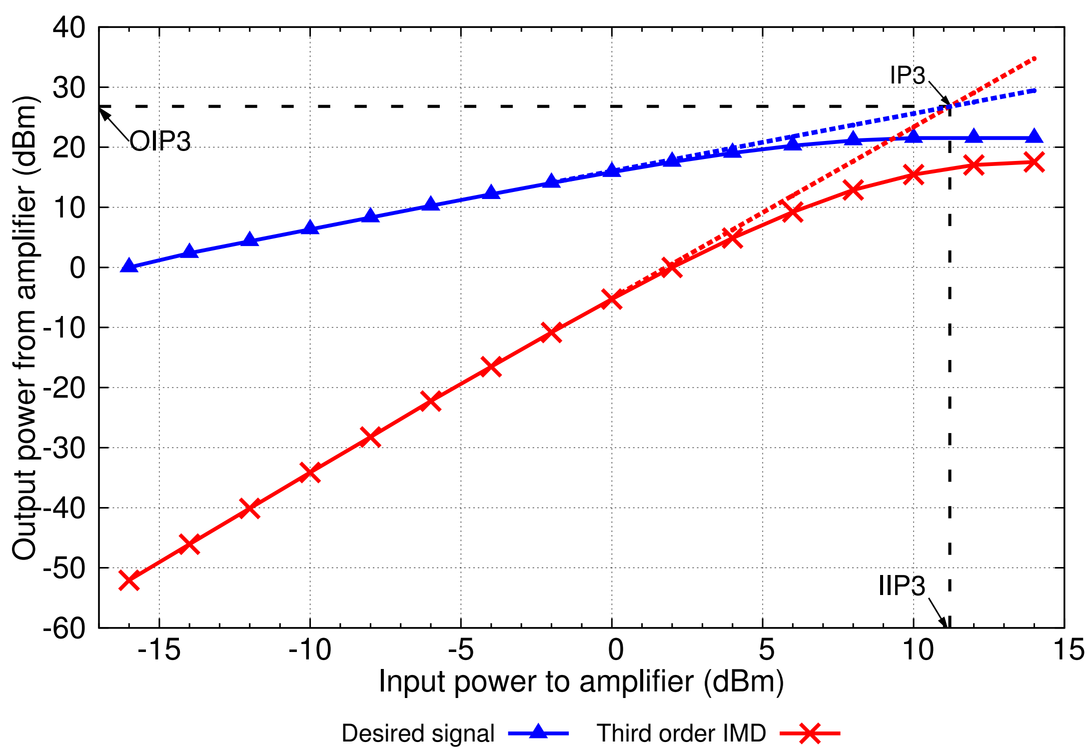

Figure 4.4. Input/output of two-tone signal and IMD distortion

4.3. The Proposed Dynamic Channel Allocation Scheme with Predistortion in Multi-channel System

4.3.1 Dynamic Channel Allocation (DCA)

Recently, various approaches have been proposed to reduce the IMD. One of the candidates is the DCA. The algorithm aims to achieve the maximum spectral efficiency by allocating appropriate channels to the RAUs. The purpose is to avoid co-channel interference and IMD among the cells in the network. The DCA algorithms, which can improve the resource utilization, have been proposed in [38, 39].

The IMD components generate an undesired signal that interferes with the transmission of the desired one. According to the distribution of the active frequency channels, the impact of IMD will vary. The frequency synthesizer can select the appropriate active frequency channels to minimize the interferences. In this research, we assume that the number of channels is 11. This complies with the frequency assignment as "W56", which is so named for being the center frequency of 5600 MHz, which has 11 independent channels between 5500 MHz to 5700 MHz using 20 MHz frequency spacing [2].

The proposed DCA algorithm aims to find the maximum value of the average carrier to distortion plus noise power ratio (CDNR) over all the active channels. The CDNR over channel i (f_i) represents the ratio of the desired signal power ($P_{Desired\,RF}$) to the IMD (P_{IMD}) plus noise power (P_{Noise}) in the same channel. This means that when the IMD power increases, the CDNR decreases, and vice versa, which is based on

$$CDNR(f_i) = \frac{P_{Desired\,RF}(f_i)}{P_{IMD}(f_i) + P_{Noise}}. \tag{4.6}$$

The noise power of the radio receiver is a thermal noise. The thermal noise power of the 1Hz bandwidth at room temperature (20℃) is −174 dBm. Since the bandwidth for each 802.11 signal is 20 MHz, the value of thermal noise is −101 dBm. In this work, we assume the value of 10 dB as the noise figure of the receiver. Hence, the noise power is −91 dBm.

The proposed DCA will calculate all CDNR values for all the possible combinations of the selected channels. The best combination that has the highest average CDNR, and minimizes the effect of IMD, is assigned to the set of active channels. Here, the vector H representing all channels is represented as

$$H = [h_1, h_2, \ldots, h_{11}] \tag{4.7}$$

and

$$h_i = \begin{cases} 1, & \text{if } i\text{-th channel is active;} \\ 0, & \text{if } i\text{-th channel is inactive.} \end{cases} \tag{4.8}$$

Suppose that an index set as $C = \{i,\ h_i = 1\}$ and the number of elements in C is M as $C_1 \ldots C_M$, where M is the number of active RF channel carriers. The average CDNR can be calculated by

$$\overline{CDNR}(H(C)) = \frac{1}{M} \sum_{i=C_1}^{C_M} (CDNR(f_i)). \tag{4.9}$$

Hence, the proposed DCA algorithm, to find the best channel combination (C_{best}), can be expressed by

$$C_{best} = \arg\max_{C} (\overline{CDNR}(H(C))). \tag{4.10}$$

We use an example to explain our DCA method. Assuming that 5 of 11 channels are active. An example of the best channel combination is shown in Fig. 4.5 using the parameters in Table 4.1.

To evaluate the CDNR at the receiving side, we assume that the distance between the RAU and the mobile station is 30 meters. The propagation loss model is the log-distance path loss model [40], which generates a loss of 88.9 dB. Each channel connects with one mobile station. The CL between the uplink and the downlink antennas is assumed to be 10, 20 and 30 dB. Due to the WiFi system, the RAU transmission power in the downlink and the mobile transmission power in the uplink are also the same as +16 dBm. The points for calculating the average CDNR are at the mobile stations for cases of the downlink, and after the uplink nonlinear block for cases of the uplink.

Table 4.1. Parameters for DCA calculation

Parameter	Values
Observed bandwidth	140 MHz
Amplitude (A_m)	0.199 V
Initial phase (ϕ_m)	Uniform distribution ($0 \leq \phi_m \leq 2\pi$)
Number of active RF (M)	5
RF carrier frequency (f_m)	5500, 5520, 5540, 5620, 5680 MHz

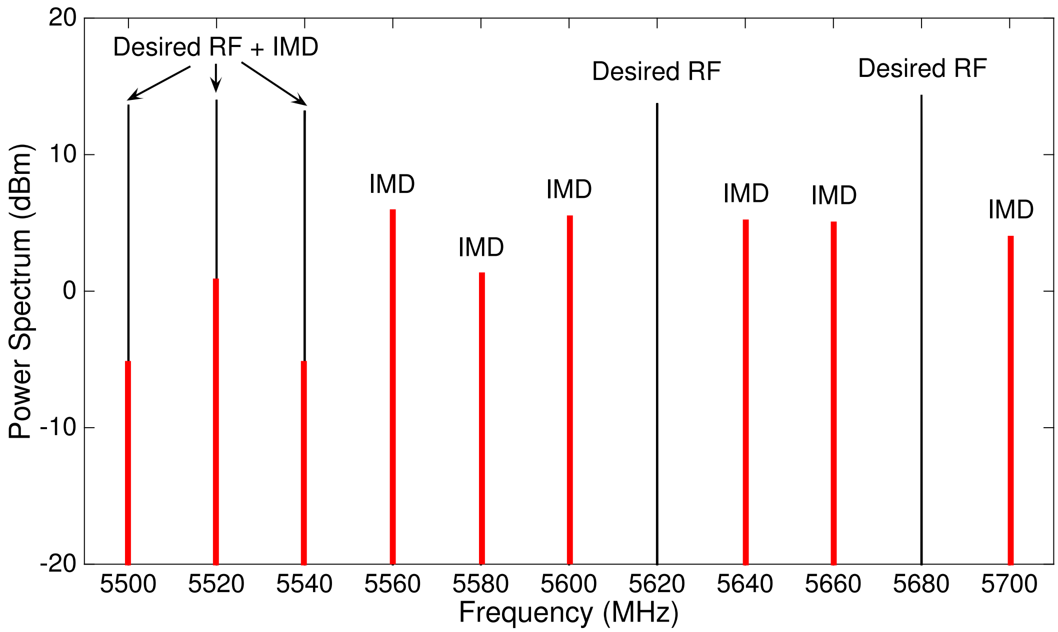

Figure 4.5. Downlink IMD after transmission through the downlink nonlinear block (marked with $\otimes$ in Fig. 4.6)

Fig. 4.6 shows the CDNR calculation of the frequency channel assignment. Due to the negligible IMD, the 18.1 dB value is the ratio of the desired signal power at the receiving side to the noise power. This means the IMD power is less than the noise power. To find the best channel combination, we use the downlink signal to calculate the highest average CDNR. From the downlink result, the low level of the IMD remains in channels 1, 2 and 3. However, the IMD does not appear at channels 7 and 10. In the uplink, we calculate the average CDNR

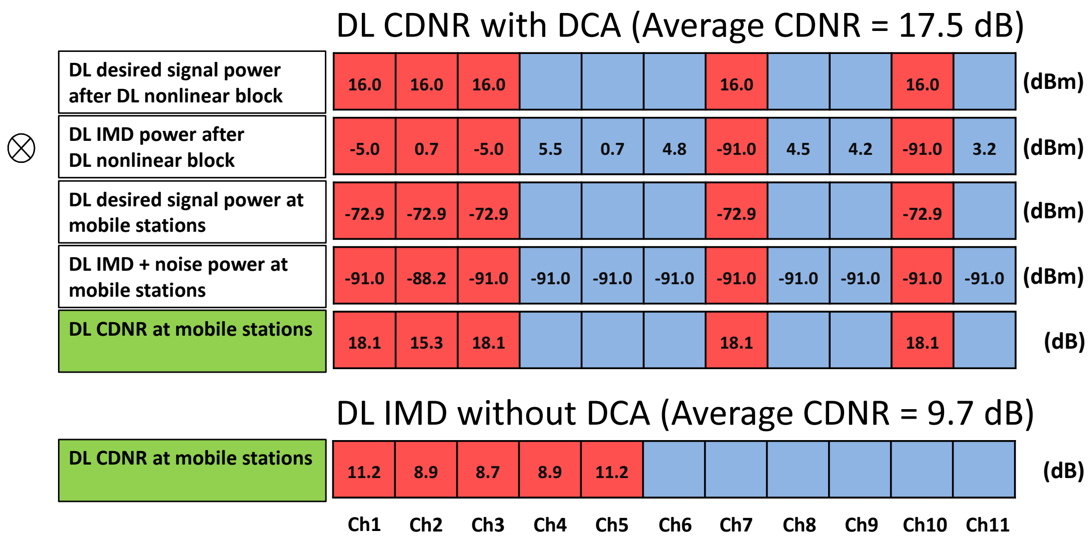

Figure 4.6. CDNR calculation for downlink, in the case of CL = 10 dB (red: downlink active, green: uplink active, blue: inactive)

taking into consideration the power difference between the downlink and the uplink signals as shown in Fig. 4.7. For example, when the channel 1 is active for the uplink signal, we assume that channels 2, 3, 7 and 10 transmit the downlink signals simultaneously, which is the worst case scenario for the uplink of channel 1. This process is repeated for the other active channels. Then we obtain the average CDNR from all of the active channels.

Fig. 4.8 shows the CDNR performance when the number of active channels is increased. In the downlink, the DCA can avoid the in-band interference in up to 4 channels, because the average CDNR increased to 18.1 dB. However, in the case of more than 4 active channels, the IMD interference remains in the desired signal, which makes the average CDNR decrease. In the uplink case with the DCA, when the number of active channels is more than 4, the CDNR deteriorates drastically due to the extremely high level of IMD as shown in Fig. 4.9. This can be alleviated by increasing the CL between the uplink and the downlink antennas. Using 30 dB of CL, the CDNR will be higher than when using 20 and 10 dB. The difference of CDNR between having the DCA and without the DCA will converge as the number of channels increases.

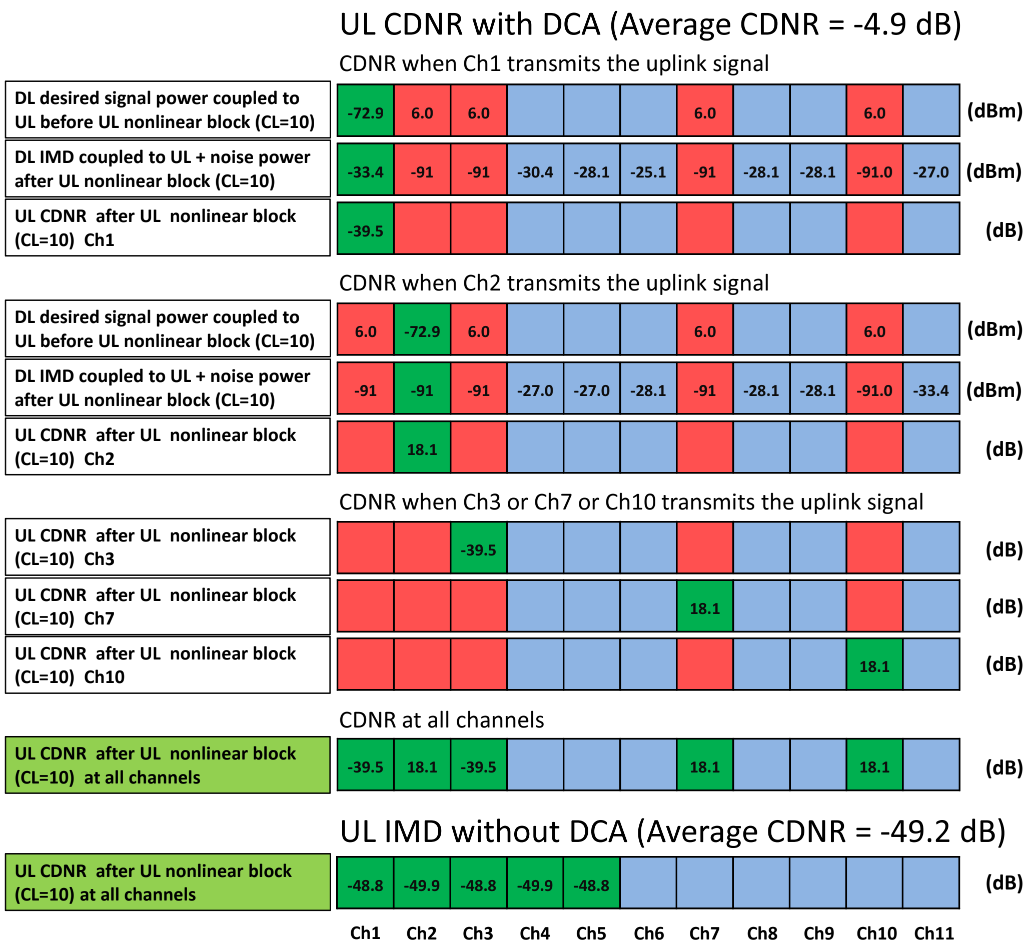

Figure 4.7. CDNR calculation for uplink, in the case of CL = 10 dB (red: downlink active, green: uplink active, blue: inactive)

Because the IMD occurs in the active channels, the number of available channels in the uplink needs to be calculated. We calculate the uplink CDNR in the same way as in Fig. 4.9. In the 802.11a, the minimum required CDNR that can achieve 10% of the packet error rates (PER) is 4.9 dB [41]. This value is then set as the threshold of the available channel. Fig. 4.10 shows the number of available channels in the uplink when the number of active channels is varied but smaller than 11. The result shows that the number of available channels in uplink will be increased by using the DCA.

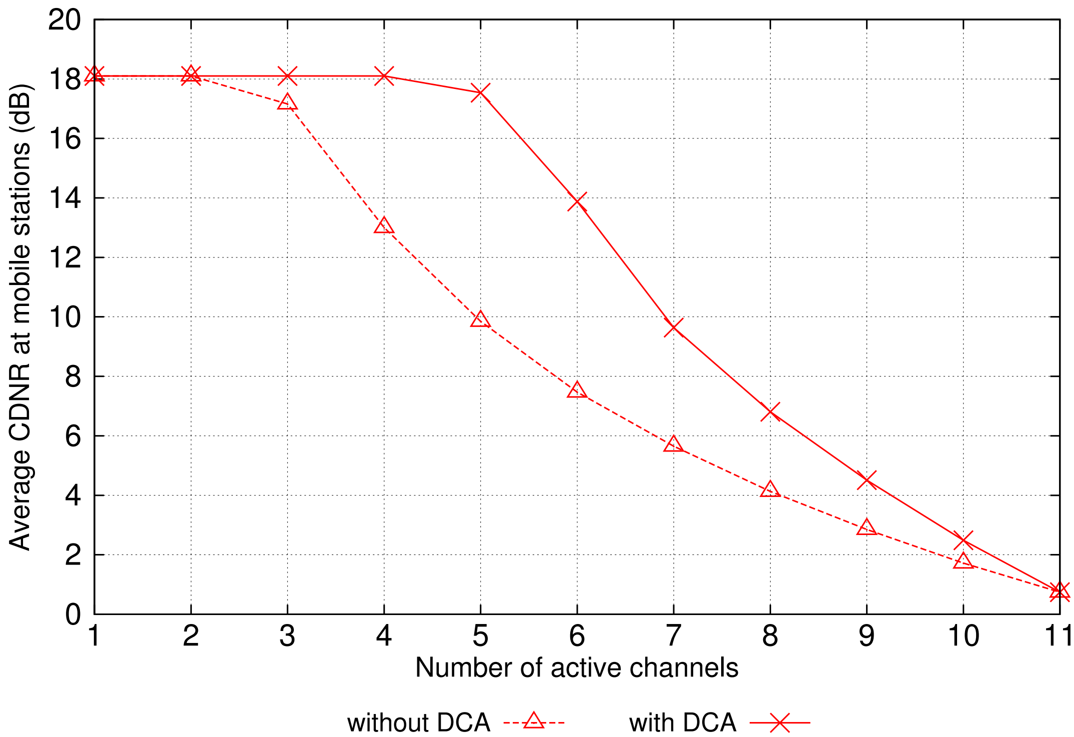

Figure 4.8. Average CDNR in downlink with the number of active channels out of 11 channels

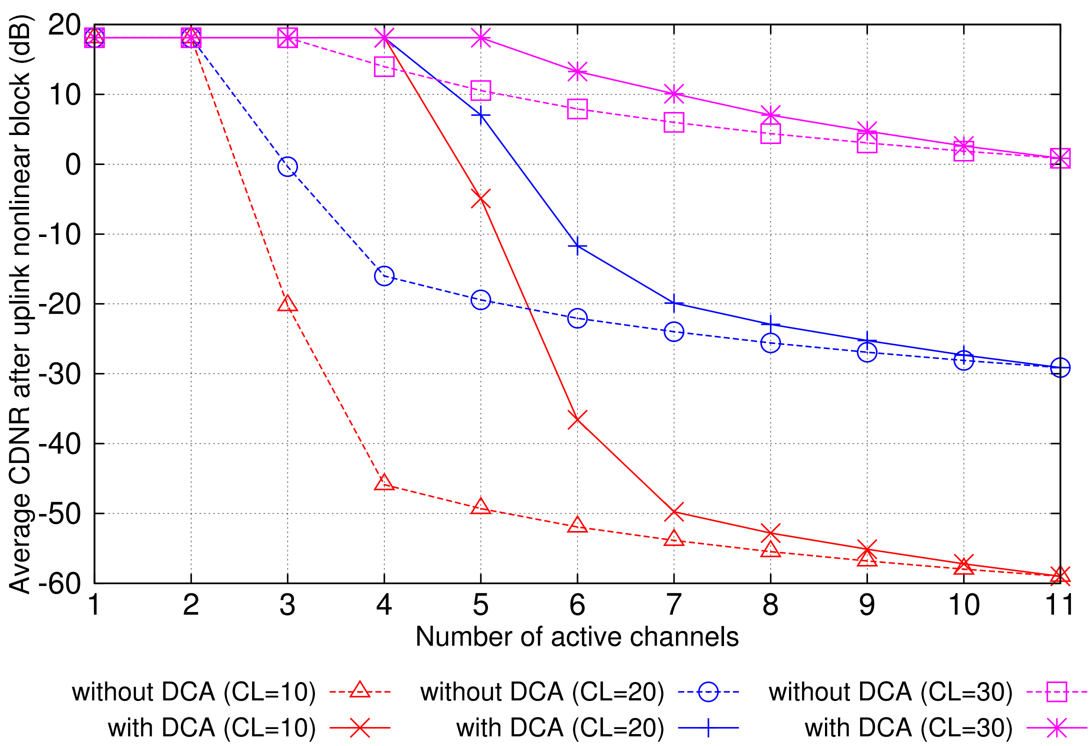

Figure 4.9. Average CDNR in uplink with the number of active channels out of 11 channels

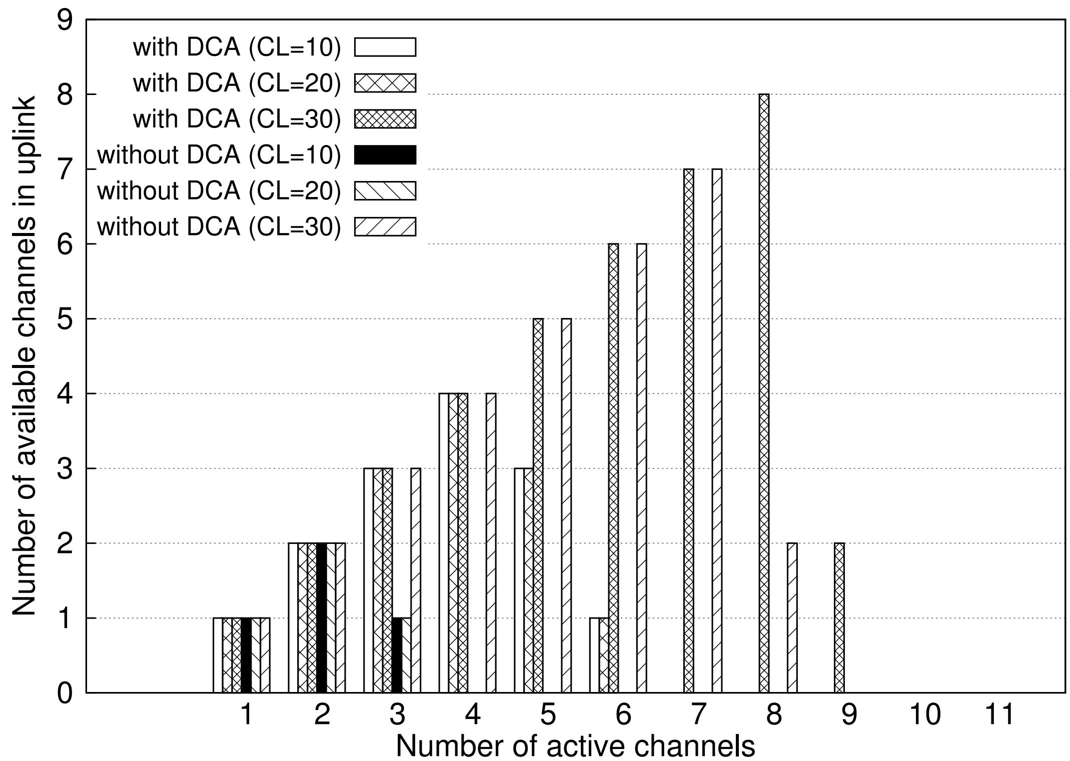

Figure 4.10. Number of available channels in the uplink with the different number of active channels

4.3.2 Predistortion (PD)

The DCA can avoid the third-order IMD in the case of few active channels. However, when the number of channels increases, the IMD will still occur and degrade the desired RF signals. Regarding this issue, the PD technique has been proposed to pre-cancel the IMD effect using the inverse characteristic of a nonlinear device. The PD can be put into two categories: the memoryless and the memory polynomial. The memoryless PD achieves a linearization performance, while the memory polynomial can model the system more accurately [12]. There are many solutions to compensate for the nonlinearity. For example, the authors of [42] presented an extension of the conventional least mean square (LMS) algorithm for the RoF, based on the memory polynomial model. Reference [43] proposed a postdistorter in the downlink transmitter. While [44] uses the uplink as a predistorter feedback, which is a more reasonable solution. Moreover, the nonlinear characteristics of PA, which vary with time, are dependent on many such factors as the amplifier's temperature, voltage variations and channel assignment. To account for all these factors, adaptive PD methods have been introduced in [45,46]. These references assert that the PD technique is one of the best candidates to compensate for the nonlinear impact for the RoF.

In the conventional PD method, an extra RoF link has been introduced as a feedback loop for the adaptive PD. The idea is to feed the uplink PA characteristic back to the RAU. However, there are many processes that need to be implemented in the feedback loop, such as loop delay calculation and equipment cost. In this work, we assume that the nonlinear from the PA in the downlink and uplink use the same Saleh model. The nonlinear characteristics of the PD can be calculated from the downlink PA, where the downlink PA and the PD are also located in the RAU.

The memory polynomial PD is used in this work because superior linearization performance can be achieved from the memory effects [12]. We use a sampled signal expression for designing the predistorter which has the memory as in [47]. The sampled signal is defined as $x_{DL}[n] = x_{DL}(nT_s)$, $x_{UL}[n] = x_{UL}(nT_s)$ and $y[n] = y(nT_s)$, where T_s is the sampling period. We assume that T_s, which is required in the analog to digital converter (ADC), has the value of 3.6 ns.

Fig. 4.11 shows the detailed block diagram of PD architecture. The PD is

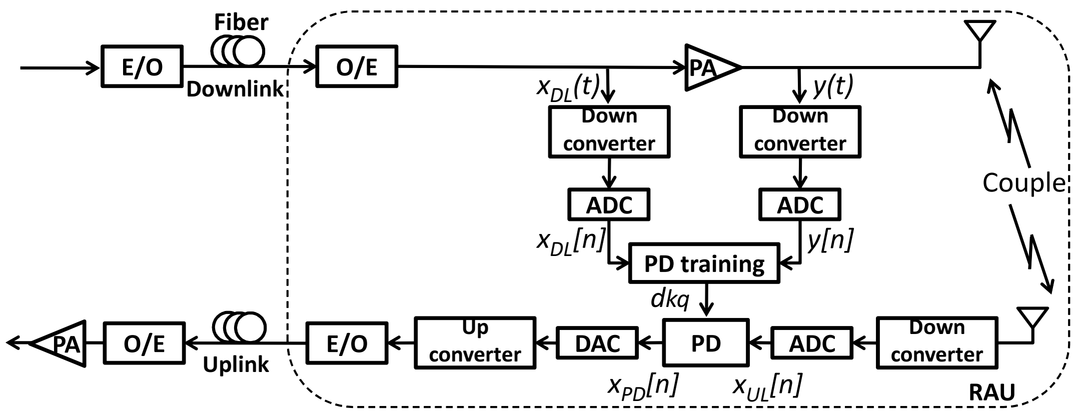

Figure 4.11. Predistortion architecture

realized using the PD training. In this training block, the $x_{DL}[n]$ and $y[n]$ signals, the prerequisites, drive the block. To find the PD coefficients d_{kq}, the memory polynomial can be used as an inverse modeling for the predistorter, which can be expressed as

$$x_{DL}[n] = \sum_{k=1}^{K} \sum_{q=0}^{Q-1} d_{kq} y[n-q] |y[n-q]|^{k-1}, \tag{4.11}$$

where K is the nonlinear order and Q is the memory length. We rewrite (4.11) as a set of linear equations as (4.12) or in matrix form as

$$X_{DL} = \Theta_Y D. \tag{4.13}$$

In this research, we used $K = 5$ and $Q = 5$ for the PD, and K times $Q = 25$ for coefficients d_{kq}. The coefficients can be estimated based on the least squares as

$$\begin{pmatrix} x_n \\ x_{n+1} \\ \vdots \\ x_{n+p} \end{pmatrix} = \begin{pmatrix} y_n & y_{n-1} & \cdots & y_{n-Q-1}|y_{n-Q-1}|^{K-1} \\ y_{n+1} & y_{n+1-1} & \cdots & y_{n+1-Q-1}|y_{n+1-Q-1}|^{K-1} \\ \vdots & \vdots & \ddots & \vdots \\ y_{n+p} & y_{n+p-1} & \cdots & y_{n+p-Q-1}|y_{n+p-Q-1}|^{K-1} \end{pmatrix} \begin{pmatrix} d_{10} \\ d_{11} \\ \vdots \\ d_{K(Q-1)} \end{pmatrix} \tag{4.12}$$

$$D = \Theta_Y^{+} X_{DL}, \tag{4.14}$$

where $\Theta_Y^{+} = (\Theta_Y^H \Theta_Y)^{-1} \Theta_Y^H$. Here H indicates the Hermitian transpose.

After the coefficients d_{kq} are obtained, the uplink input signal to the PA after the PD $x_{PD}[n]$ can be calculated by

$$x_{PD}[n] = \sum_{k=1}^{K} \sum_{q=0}^{Q-1} d_{kq} x_{UL}[n-q] |x_{UL}[n-q]|^{k-1}, \tag{4.15}$$

where $x_{UL}[n]$ is the uplink signal before the PD block. Then, the $x_{PD}[n]$ signal is converted to analog and passed to the uplink PA through the RoF link.

In this work, we assume that the nonlinear characteristics do not change rapidly with time. Therefore, there is no need for $x_{DL}[n]$ and $y[n]$ to be adaptive. After getting $x_{DL}[n]$ and $y[n]$ as the stored signals, the offline data can be processed using the PD training block. This helps reduce the PD processing time [42].

Fig. 4.12 depicts the impact of PD on the CDNR performance in uplink. The environment parameters for this simulation are also the same in Section 4.3.1, with $K = 5$ and $Q = 5$. Here, we calculate the results by altering the transmission power from 0 dBm to +16 dBm. Five channels are assigned to the contiguous channel; then the IMD compensation is calculated from the average CDNR of the active channels. The result shows that about a 6 dB increase in the CDNR value was realized when applying memory polynomial PD compensation.

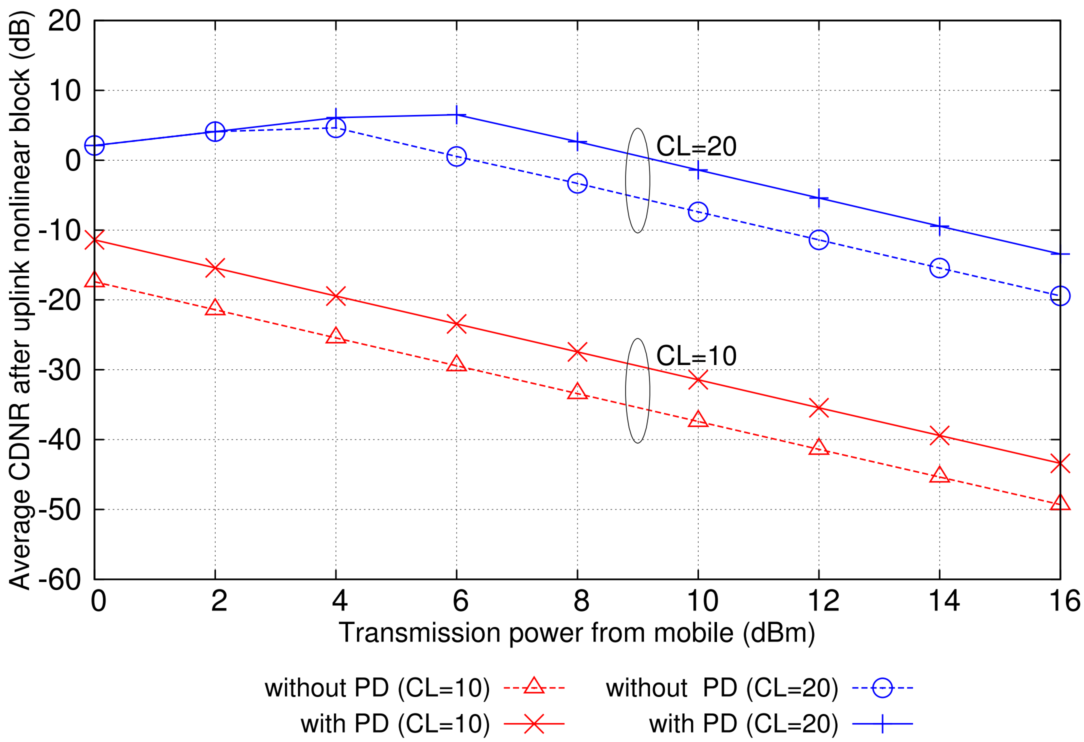

Figure 4.12. Average CDNR in the uplink when PD is applied

4.4. Combination of Dynamic Channel Allocation and Predistortion

In this section, we combine the DCA and the PD to improve the CDNR performance. In the PD process, we use $K = 5$ and $Q = 5$. The CL between the downlink and the uplink antennas in the RAU is 20 dB. The distance between the RAU and the mobile station is 30 meters, with the log-distance path loss model. The CDNR performance is calculated from the average CDNR of all the active channels.

The optimal transmission power depends on many factors, including the signal power, the CL and the number of active channels. In accordance with the WiFi system, we assume that the transmission power in the downlink and the uplink are identical. We derive an optimal power in order to determine the transmission power of the RAU and the mobile stations. Since the coupled downlink signal here is higher than the uplink signal, the optimal transmission power is decided by the uplink CDNR performance, as shown in Fig. 4.13. In the case of a low transmission power, the CDNR is reduced because of the decreasing transmission power. As for a high transmission power, the CDNR performance is degraded because the high level of IMD interferes with the desired signal. We can obtain the optimal transmission power from the curve's peak. In the case of using the DCA with the PD, the transmission power with +10 dBm can be treated as the optimal one.

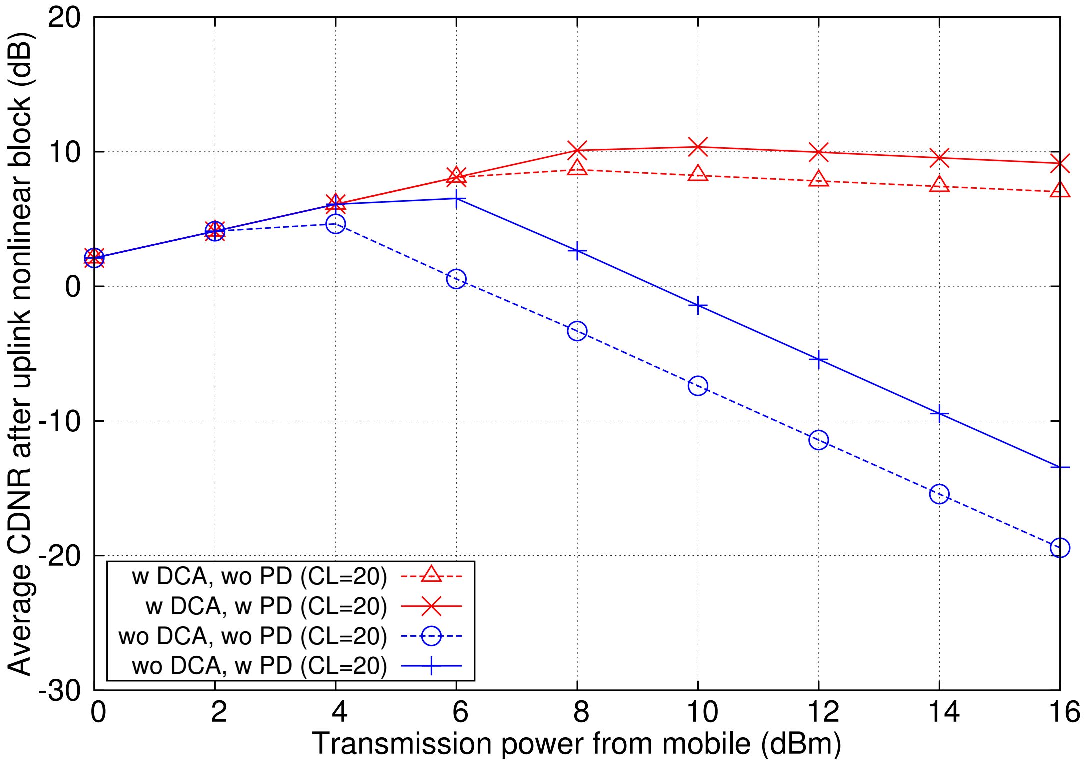

Figure 4.13. Average CDNR in the the uplink when the DCA and PD are applied

4.5. Network Simulation

According to the results in the previous sections, the theoretical calculation alone is not enough, as it assumes that the uplink and the downlink always interfere with each other. This assumption is however not correct, since the IMD does not occur all the time but instead depends on the amount of data traffic. To provide an accurate evaluation in terms of the throughput performance, this thesis introduces a network simulation that can simulate the media access control (MAC) protocol in the realistic WiFi. The multiple data links between the user and the server can be realized in the simulation, which includes the physical (PHY) layer and the MAC layer using the discrete-event network simulator version 3 (ns-3) [25].

To explain the frame transmission in the WiFi system, Fig. 4.14 shows the timeline of the IMD interference with the downlink signal. The IMD and the desired signal are simultaneously transmitted through the air interface. However, Fig. 4.15 shows the interference at mobile station, the IMD power is less than the transmitted signal power.

Fig. 4.16 shows the uplink transmission timeline after the nonlinear block in the CCS. When the uplink signal and the coupled downlink signals are transmitted through the fiber-optic link, the IMD will occur at the output of the nonlinear block in the CCS. This IMD occurrence can be considered to be one reason for the throughput deterioration. Moreover, as shown Fig. 4.17, we have considered such cases of "no interference" and "partial interference" in the simulation. In both cases, the IMD will occur depending on the time variation.

To demonstrate the effectiveness of the DCA and the PD, the throughput

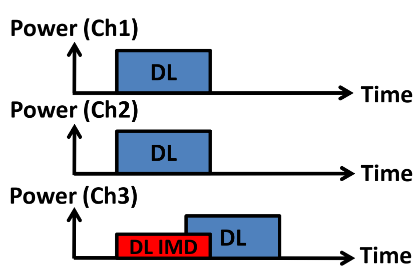

Figure 4.14. Downlink transmission timeline at RAU

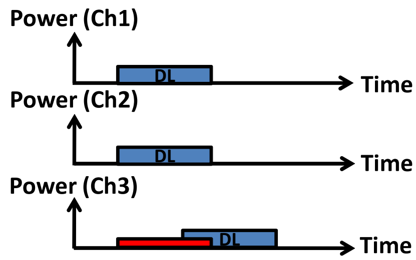

Figure 4.15. Downlink transmission timeline at mobile station

performance is evaluated. Table 4.2 shows the simulation parameters, and the experiment scenario is presented in Fig. 4.18. We use the total uplink throughput, which is summed from the successfully transmitted data per second in the uplink, as the metric of the simulation. Assuming that 5 channels are selected out of 11 based on the proposed DCA, and each active channel is shared by 5 mobile stations. All of 25 mobile stations send the data to the server via the RAU. Since we assume that the offered load for each mobile station is 1 Mbps, the maximum value of the total uplink throughput is 25 Mbps. The mobile stations are randomly placed in a two-dimensional circle. The RAU is at the center of the circle, and the diameter of the circle is 100 meters.

Due to the acknowledgment procedure of the RTS and the CTS, the IMD can affect not only the uplink data flow but also the downlink flow (RTS: Request to send, CTS: Clear to send). This means that even if the data are transmitted from

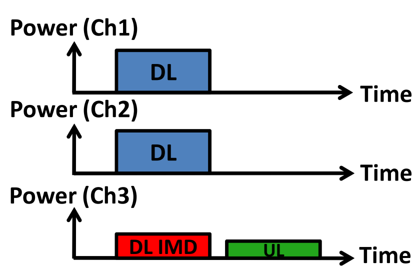

Figure 4.16. Uplink transmission timeline after the nonlinear block in CCS without interference

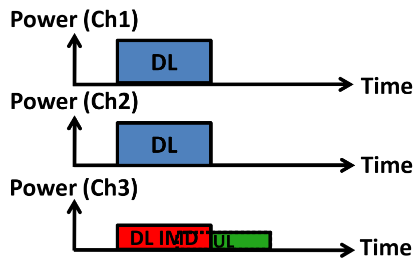

Figure 4.17. Uplink transmission timeline after the nonlinear block in CCS with partial interference

the RAU to the mobile stations in the downlink flow, the uplink path is still used as the path to send the acknowledgment data (CTS). However, in order to analyze the uplink performance, the uplink flow throughput results are investigated.

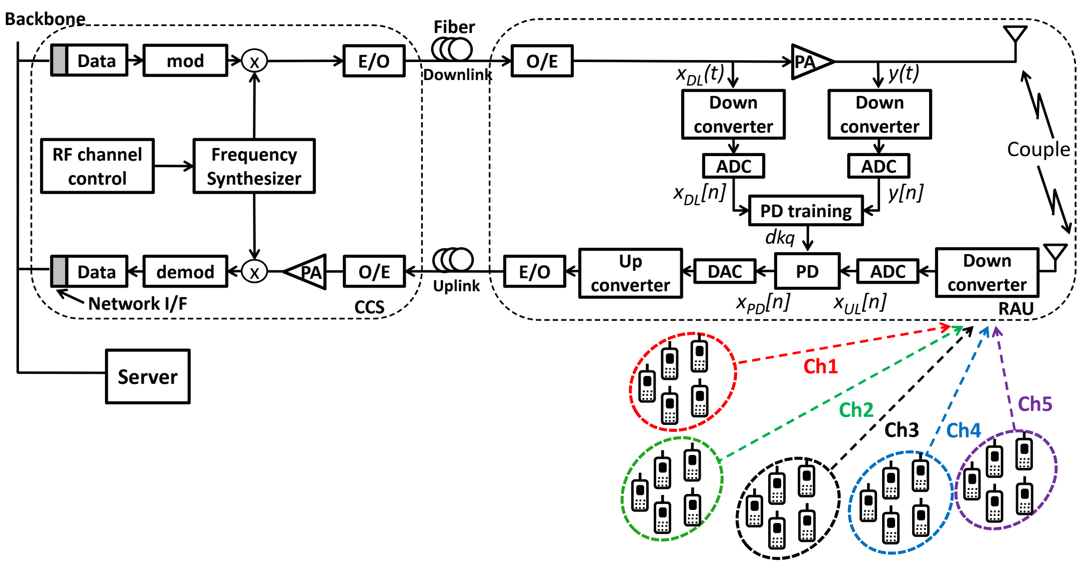

Figure 4.18. Scenario in the network simulation

Table 4.2. Simulation parameters in the network simulation

Parameter	Values
Radio standard	802.11a
Offered load for each mobile station	1 Mbps
Application type	On-Off application (UDP)
Packet size	1024 bytes
Tx power to the DL nonlinear block	+8 dBm
Tx power from the mobile station	+8 dBm
Number of active channels	5 channels (with DCA, without DCA)
Number of mobile stations per channel	5 stations
Total number of mobile stations	25 stations
Mobility model of the mobile stations	RandomWalk2dMobilityModel [27]
Mobility speed of the mobile stations	1.5m/s (Assumed for walking person)
Propagation loss model	LogDistancePropagationLossModel [40]
Propagation delay	ConstantSpeedPropagationDelayModel [26]
PD polynomial order (K)	5
PD memory length (Q)	5
Coupling loss (CL) (between the downlink and the uplink antennas in the RAU)	10, 20, 30 dB

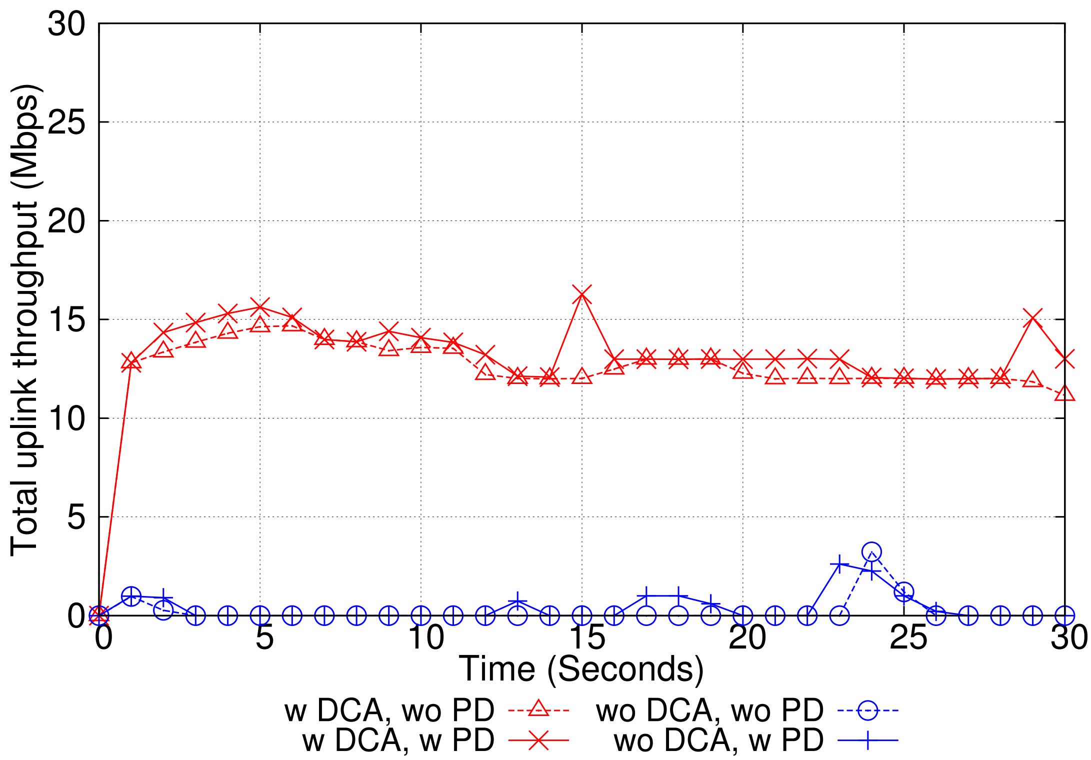

Figure 4.19. Uplink throughput performance (CL = 10 dB)

Fig. 4.19 shows the total throughput of the system when the CL between the downlink and the uplink antennas is 10 dB. If the DCA is not used, the mobile stations can send a few data, since the IMD from the coupled downlink signal power is higher than the uplink signal in all active channels. However, using the DCA, some of the mobile stations are capable of sending the data over the RoF link, because the IMD is not present in some channels, as shown in Fig. 4.7. In the cases of using the memory polynomial PD, the PD will result in low effect in terms of throughput, due to the high level of the coupled downlink signal. In the case that CL = 10 dB, we can conclude that using PD alone is not an effective way to improve the throughput performance.

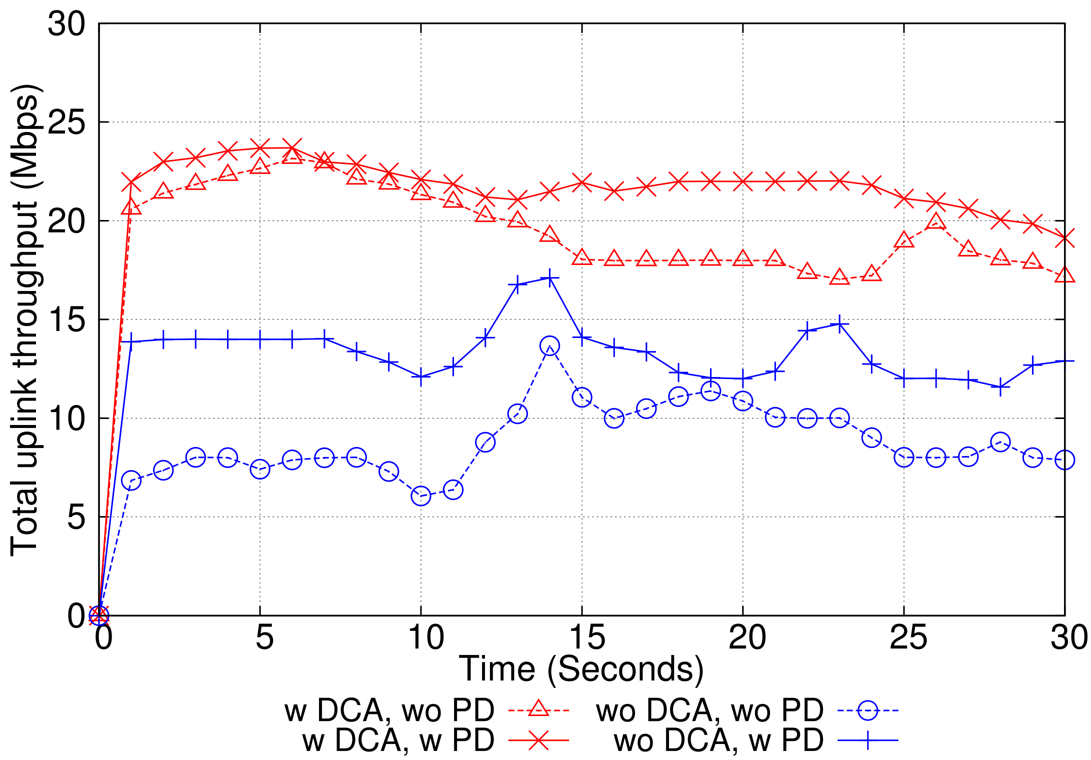

Figure 4.20. Uplink throughput performance (CL = 20 dB)

From Fig. 4.20, when the CL is 20 dB, we can see that the DCA with the lowest IMD achieves the best performance regardless of the station's velocity. Moreover, the PD has a considerably increased throughput. However, without DCA, the throughput decreases because the IMD increases the interference of the desired signal.

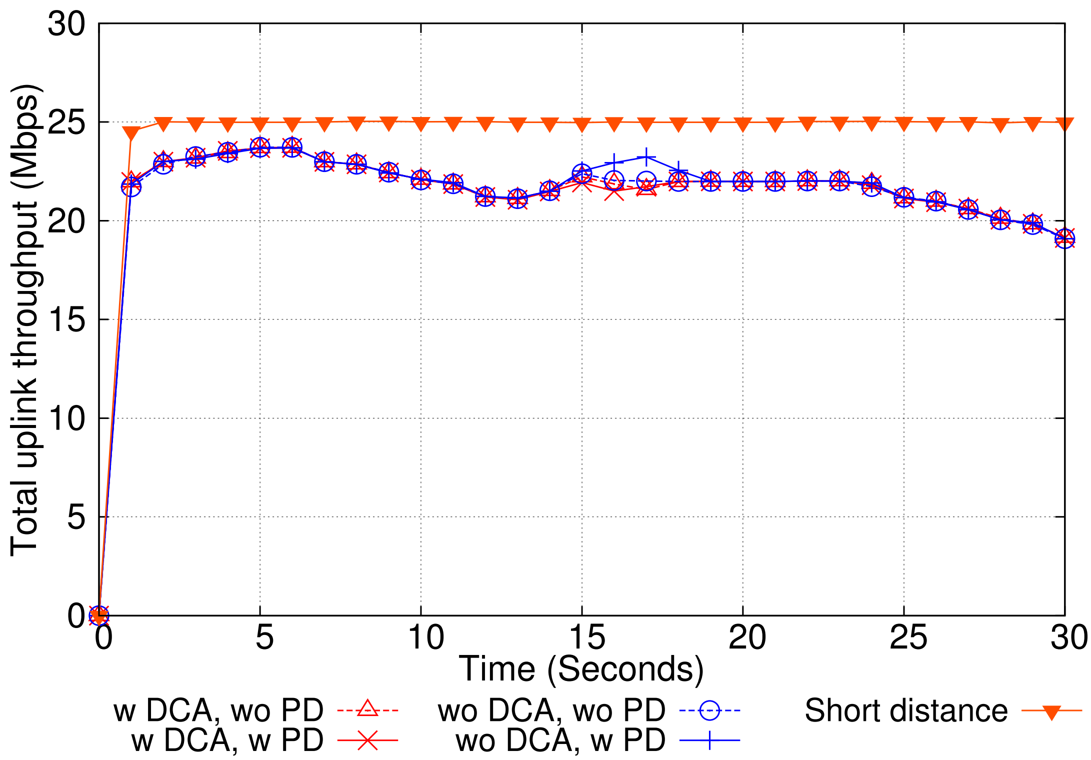

Figure 4.21. Uplink throughput performance (CL = 30 dB)

The results for CL = 30 dB are shown in Fig. 4.21. The throughput performance is almost the same for every case because of the high value of the CL, which reduced the IMD to less than the noise power. To confirm that the decrease in the throughput does not occur due to the IMD, we also provide the result for the case of a short distance, for which the DCA and PD are not used. For that purpose, the diameter of the circle of the user's location is reduced from 100 to 30 meters. The result shows that the gap between the two distances is due to the different path loss distance.

We can conclude that our channel allocation scheme can perform well in the cases of CL = 10 and 20 dB. Its throughput performance can be further improved by using PD. However, as the CL is increased to more than 30 dB, the improvement provided by our channel allocation scheme together with the PD becomes less significant since the IMD is extremely low.

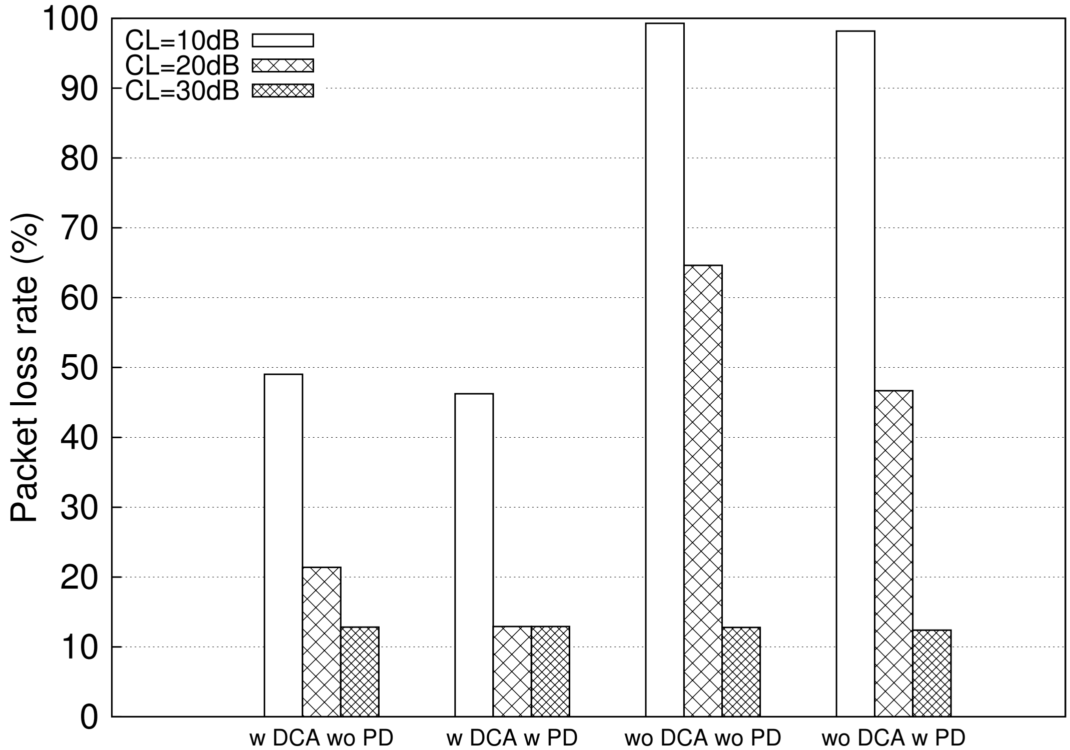

Figure 4.22. Uplink packet loss rate

The performance of the packet loss rate related to the IMD is shown in Fig. 4.22, which defines the packet loss rate as the ratio of the lost packets to the transmitted packets. The result shows that the DCA with PD has a low packet loss rate. In contrast, the packet loss is high when the DCA is not used. Therefore, our proposal using the DCA and PD is an effective method to reduce the impact of IMD interference.

4.6. Conclusion

In this research, the problem of the IMD interference between the uplink and the downlink in the multi-channel RoF system has been addressed. From our experiments, the coupled downlink signal interferes with the uplink signal and results in the degradation of system performance when the antenna coupling is less than 30 dB. To mitigate the IMD, we propose using the DCA in conjunction with the PD technique. The memory polynomial model was used to model the PD. From the results of using the DCA with the PD, the optimal transmission power was obtained. Moreover, we confirmed that our proposal can improve the throughput performance in the realistic WiFi by using the network simulation.

Chapter 5

Final Remarks

5.1. Conclusion

Nowadays, many services providers have already implemented RoF in order to support the growing traffic requirement. Classified by the type of the transmission, RoF can be categorized into two configurations: digitized RoF and analog RoF. Due to the problems concerning nonlinearity and noise tolerance can be easily found in the analog RoF, many researchers want to move the RoF configuration from analog to digital by applying the CPRI protocol. However, the next generation of the communication system required about 100 Gbps of the link transmission rate, assuming that three sectors using 16x16 MIMO with 20 MHz of LTE-A signal are implemented. Since then, more focus is given back to the analog RoF with the additional configuration such as WDM. Therefore, this thesis emphasizes on the performance enhancement of the C-RAN with analog RoF system. First, the handover reduction scheme over C-RAN configuration is introduced. Second, we proposed the method to alleviate the nonlinearity.

The first part of the study, Chapter 3, is about the handover reduction scheme for C-RAN configuration. Since the conventional mobile backhaul is based on the CPRI point-to-point link, the handover process needs to be activated whenever the mobile station moves across the cell. However, this problem can be alleviated by using the C-RAN with analog RoF. According to this benefit, we proposed an algorithm to group the neighboring nodes together, which the controller can gather all of the information without using additional protocols. Our proposal can drastically decrease the number of handover compared with the point-to-point configuration, which is about 38.27 % when the user's speed is 2 m/s.

In the second part of the study, Chapter 4, the effect of nonlinearity from RoF devices was studied in the context of the multi-channel communication system since it has not been reported to date. This kind of IMD interference has a high effect in the uplink direction when CL between downlink and uplink is low. We proposed two methods using the DCA with the PD technique which aims to reduce the IMD in link-level. From the results, we found that our proposal could perform well in the cases of CL = 10 and 20 dB. Its throughput performance can be further improved by using PD. However, when the CL is increased to more than 30 dB, the improvement from our proposal becomes less significant since the IMD is extremely low.

5.2. Future Work

Recently, the C-RAN with analog RoF fiber is a requirement of the future mobile networks. Other important and interesting direction is to further study the practical mobile communication system since the femtocell and macrocell networks are integrated together. The cooperative radio resource management among the different wireless technologies need to be considered. To aim for even greater improvement of the performance, in our view, the complexity of handover reduction algorithm should be based on the user velocity and its direction. Moreover, in the part of channel allocation, the experiments of the IMD effect should be carefully investigated because the commercial LTE has several bands with different bandwidth and some operators utilize multiple bands. These scenarios make the algorithm more complex, and their performance has not been reported to date.

Appendix

In this chapter, we analyzed the coupling loss (CL) effect that related to the Chapter 4. The network analyzer was used to confirm the CL results by increasing the distance between Tx and Rx antennas compared with the theoretical result. Moreover, in order to analyze the effect of polarization, we also change the cosine factor of an angle between the RF antennas. We use S-Parameters as a factor to analyze the CL effect, which the details and experiments are shown as following subsections.

S-Parameters

S-Parameters is a mathematical form that represents RF energy transmits through a multi-port network, which is commonly used for an N-port network. Generally, "N-port" networks in microwave transmission are one-port and two-ports. S-Parameters are constructed in a matrix format, which the number of rows and columns are the number of ports as shown in (5.1) and (5.2).

$$\begin{pmatrix} S_{11} \end{pmatrix} \text{(one-port)} \tag{5.1}$$

$$\begin{pmatrix} S_{11} & S_{12} \\ S_{21} & S_{22} \end{pmatrix} \text{(two-ports)} \tag{5.2}$$

The S-Parameters matrix for an N-port illustrates N^2 coefficients; each value represents the input and output paths. For example, in the case of two-ports, the S_{12} represents the power transferred from port 1 to port 2. Conversely, S_{21} means the response at port 2 due to a signal at port 1. Thus S_{11} refers to the

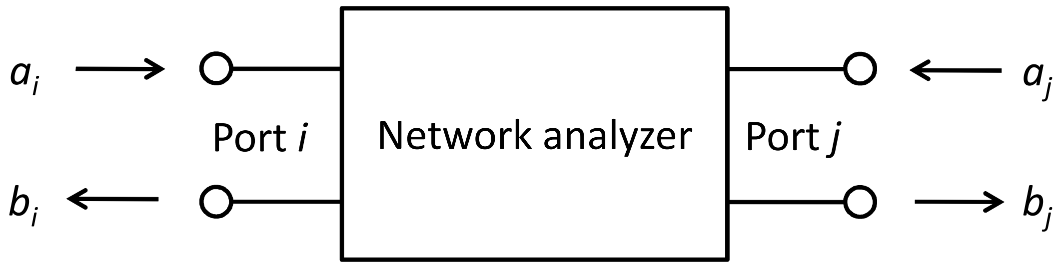

Figure 5.1. Logical two-port of network analyzer

ratio of the amplitude of signal that reflected from port 1 to the signal incident on the same port.

From Fig. 5.1, the variable a_i means a wave goes into port i and b_i represents a wave reflected from port i. We can assume the S-Parameters of the two-port as follows:

$$S_{11} = b_1/a_1 \tag{5.3}$$

$$S_{12} = b_1/a_2 \tag{5.4}$$

$$S_{21} = b_2/a_1 \tag{5.5}$$

$$S_{22} = b_2/a_2. \tag{5.6}$$

Here, we use S-Parameters in (5.3), (5.4), (5.5) and (5.6) to observe the loss between two antennas. For example, $S_{21} = -10$ dB, if the signal power of 30 dBm (1 Watt) is transmitted from antenna 1, then the power of 20 dBm (0.1 Watt) is received at antenna 2.

Antenna Polarization

The effect of polarization can be caused by the linear or circular polarization, depending on the design of an antenna. Theoretically, the polarization loss (F) between the antenna and a perfect wave plane is given by

$$F = 1 - \cos^2(\Theta), \tag{5.7}$$

where Θ is the angle between the wave plane and the antenna plane. However, in the real practice, the perfect wave plane will not occur; the reflection changes from the plane polarization to the elliptical polarization. The polarization loss is increased by the number of reflections. Therefore, the maximum signal coupling occurs when the transmitting and receiving antennas are using the same polarization. In the linearly polarized system, the polarization loss from the different of 45° between the antennas can increase the CL about 3 dB. While the different of 80° can result in more than 20 dB of the CL [48].

Fig. 5.2 shows the polarization relation between the transmitting and receiving antennas, where E_t is the transmitted polarized electric field caused by the transmitting antenna and E_r represents the electric field at the receiving antenna. The angle T_t is the tilt angle of the transmitted field, and T_r is the tilt angle of the received field. The relationship between these angles is shown as follows:

$$T_r = 180 - T_t. \tag{5.8}$$

Due to the polarization alignment between the transmitting and receiving

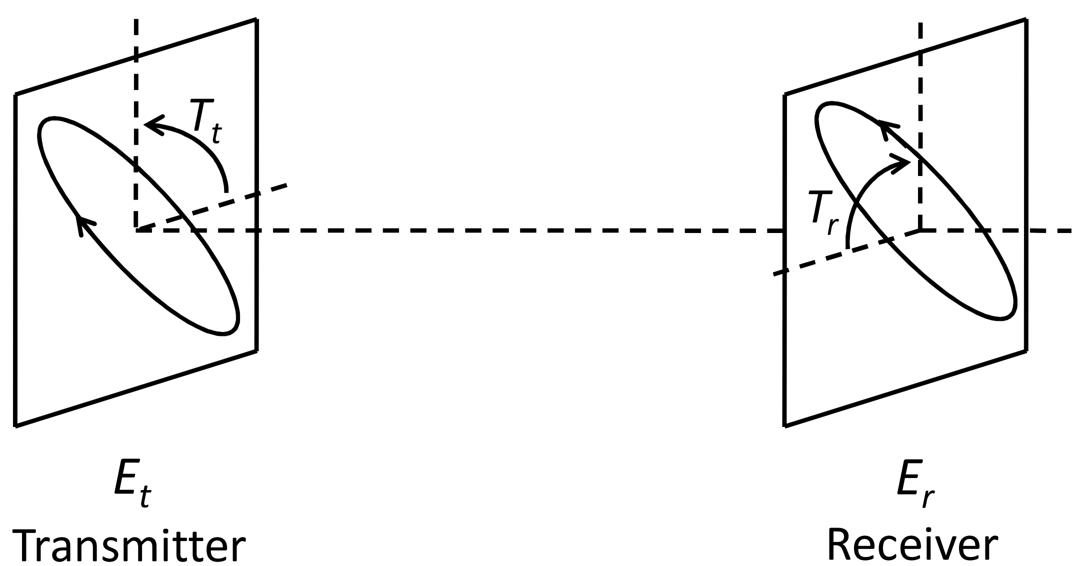

Figure 5.2. Polarization relation between the transmitting and receiving antennas

antennas is different, the polarization mismatch can occur. The relative power level of the electric field that captured from the receiving antenna is theoretically explained as shown in the following equation,

$$E_r = 20\log(\cos(T_r)). \tag{5.9}$$

Coupling loss Experiments

In this section, we designed the experiments as shown in Fig. 5.3. Two antennas are connected to network analyzer via port 1 and port 2. We investigated the CL by changing the distance (D) and angle (Θ) between two antennas. Moreover, we also compare the results with the theoretical analysis from the Friis model.

The Friis model was used in the telecommunication engineering and presented the power received at antenna under the free-space ideal condition. The Friis model equation is shown as follows:

$$\frac{P_r}{P_t} = G_r G_t \left(\frac{\lambda}{4\pi D}\right)^2, \tag{5.10}$$

where P_r is the input of the receiving antenna, P_t is the output from the transmitting antenna, λ is the wavelength, D is the distance between the antennas, G_r and G_t represent the antenna gains of the receiving and transmitting antennas, respectively. In this experiment, we use the half-wave dipole antenna as for the receiving and transmitting antennas, hence, the G_r and G_t would be 1.64 [49]. We analyzed the center frequencies of 2.4 GHz and 5.6 GHz by changing the value in network analyzer, which the λ of 2.4 GHz is equal to 0.0625 meters and λ of 5.6 GHz is 0.0267 meters due to the half-wave dipole effect.

Fig. 5.4 shows the CL result using the center frequency of 2.4 GHz. When the angle between antennas is 90°, the high level of CL can be observed due to the antenna polarization effect. Moreover, the result of 0° and theoretical model are almost the same. Hence, we can conclude that our experiment was done correctly, and the CL can be increased using the effect of antenna polarization. The results for the center frequency of 5.6 GHz are shown in Fig. 5.5. The CL of 90° polarization is highest, compared with the other. Due to the results using the center frequency of 5.6 GHz from Fig. 4.21 in Chapter 4.5, we conclude that when the CL is increased to more than 30 dB, the improvement provided by the DCA together with the PD becomes less significant since the IMD is extremely low. The theoretical model results in 25 dB of CL when the distance between antennas is 0.0625 meters, which means when the distance between the antennas is less than 0.0625 meters, the IMD still exists and interferes to the uplink desired signal. However, the theoretical analysis results in different from our experiments trend. To find out why this results happened, we have analyzed the S_{11} in order to investigate the reflected signal from an antenna that we used as shown in Fig. 5.6 and Fig. 5.7. If the S_{11} is equal to 0 dB, then all of the power is reflected from the antenna which means nothing is transmitted. As shown in Fig. 5.6, if S_{11} is equal to -20.241 dB, this implies that if 10 dBm of power is transmitted to the antenna, -10.241 dBm is the reflected power. By compared the S_{11} results of using 2.4 GHz and 5.6 GHz, we can conclude that the antenna that we used was designed for using of 2.4 GHz center frequency. This is the reason why the theoretical analysis in Fig. 5.5 is different from the results that we tested.

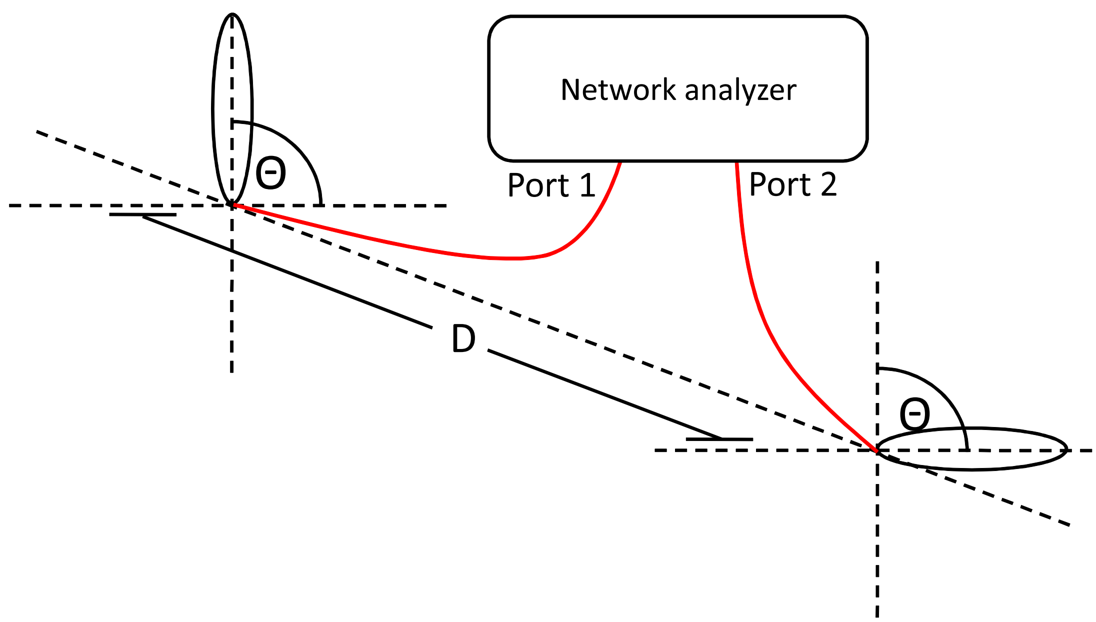

Figure 5.3. Coupling loss experiment scenario

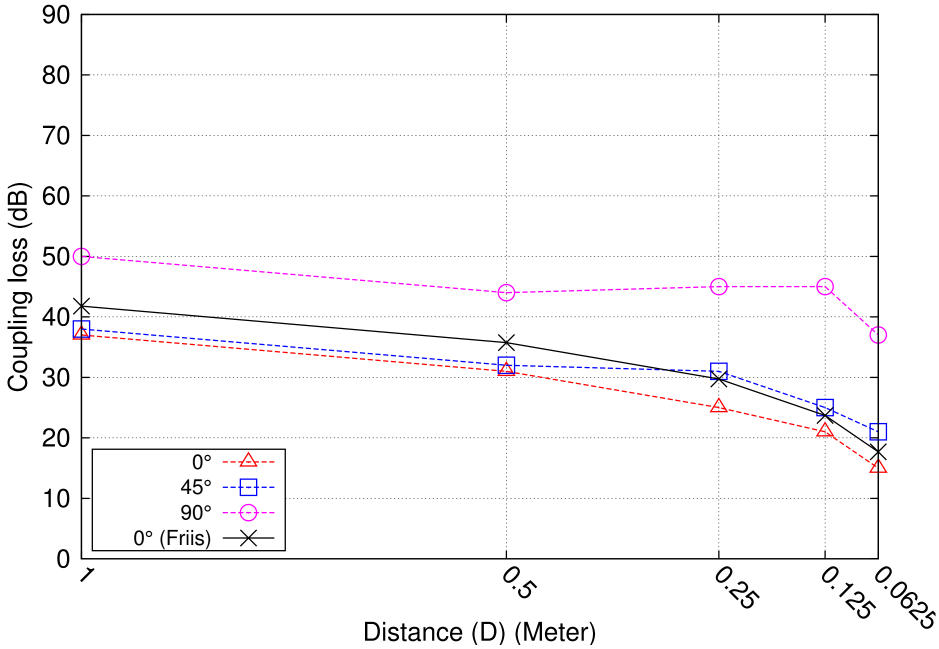

Figure 5.4. CL results using center frequency of 2.4 GHz

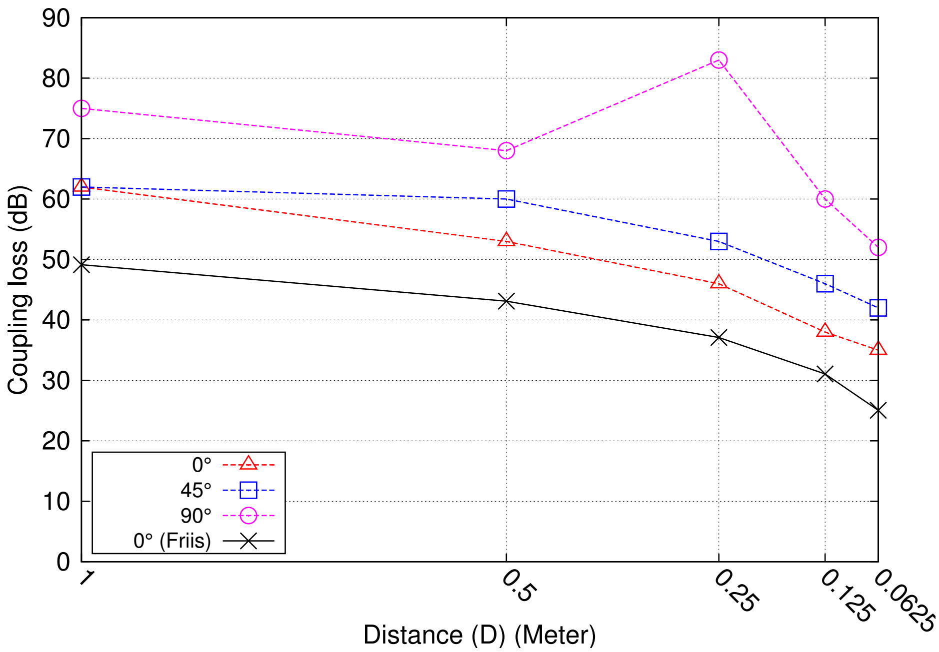

Figure 5.5. CL results using center frequency of 5.6 GHz

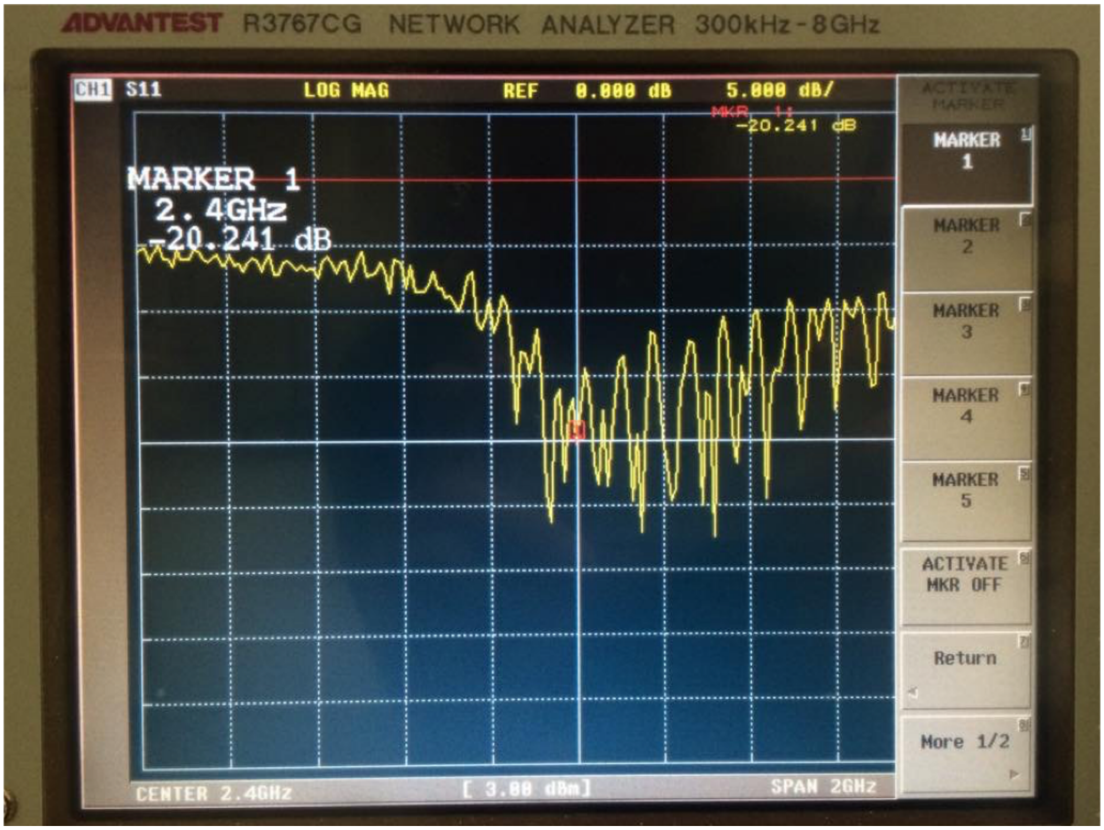

Figure 5.6. S_{11} (Return loss) using center frequency of 2.4 GHz

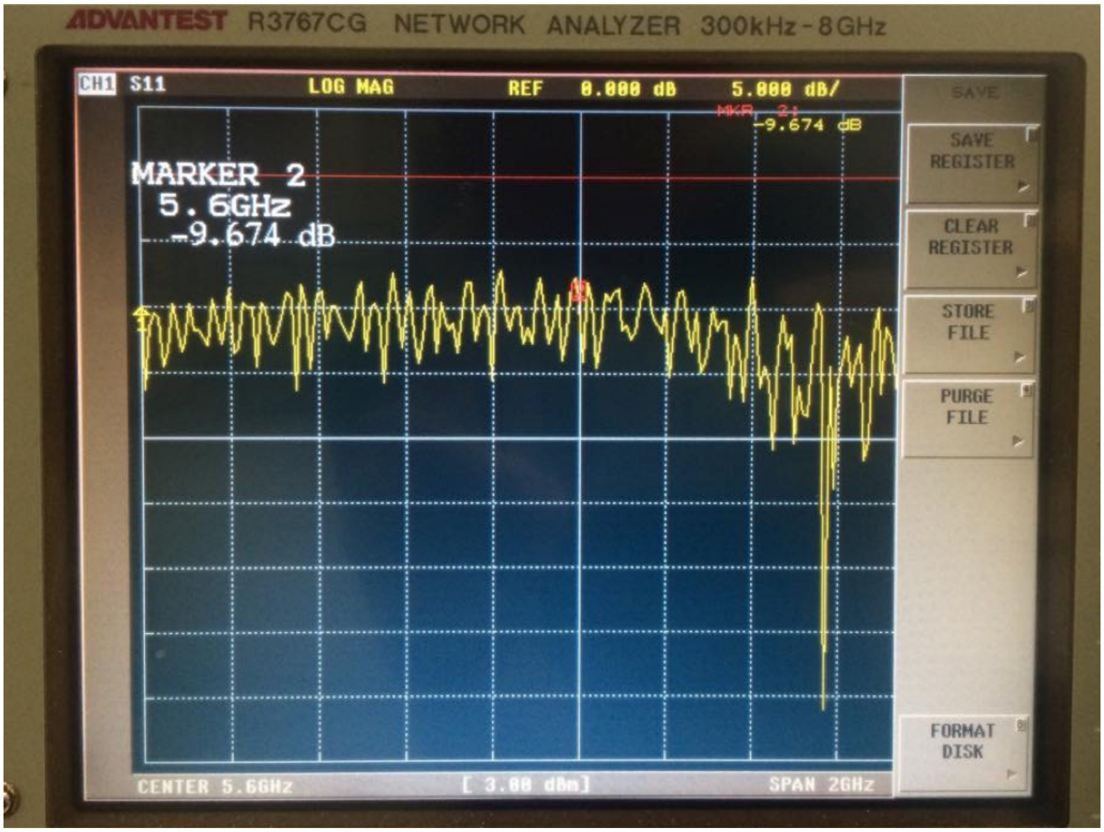

Figure 5.7. S_{11} (Return loss) using center frequency of 5.6 GHz

References

[1] T. Niiho, M. Nakas, K. Masuda, H. Sasai, K. Utsumi, and M. Fuse, "Transmission performance of multichannel wireless lan system based on radio-over-fiber techniques," *Microwave Theory and Techniques, IEEE Transactions on*, vol. 54, pp. 980–989, Feb 2006.

[2] ARIB, "Broadband Mobile Access Communication System (STD-T71)," tech. rep., October 2015.

[3] A. J. Cooper, "Fibre/radio for the provision of cordless/mobile telephony services in the access network," *Electronics Letters*, vol. 26, pp. 2054–2056, Nov 1990.

[4] ITU, "Radio-over-fibre (RoF) technologies and their applications," tech. rep., July 2015.

[5] K. Tanaka and A. Agata, "Next-generation optical access networks for c-ran," in *Optical Fiber Communications Conference and Exhibition (OFC), 2015*, pp. 1–3, March 2015.

[6] A. Agata and S. Nanba, "Optical Access Technologies for Efficient Deployment of Next Generation Cellular Networks," tech. rep., June 2015.

[7] M. Arief, S. M. Idrus, and S. Alifah, "The scm/wdm system model for radio over fiber communication link," in *RF and Microwave Conference, 2008. RFM 2008. IEEE International*, pp. 344–347, Dec 2008.

[8] R. L. Davies and F. E. Gentry, "Control of electric field at the surface of p-n junctions," *IEEE Transactions on Electron Devices*, vol. 11, pp. 313–323, Jul 1964.

[9] EMCORE, "RF and Microwave Fiber-Optic Design Guide," tech. rep., ORTEL, 2003.

[10] T. Mizumoto, R. Takei, and Y. Shoji, "Waveguide optical isolators for integrated optics," *IEEE Journal of Quantum Electronics*, vol. 48, pp. 252–260, Feb 2012.

[11] Ericsson AB, Huawei Technologies, Alcatel Lucent, and Nokia Siemens Networks, "Common Public Radio Interface (CPRI); Interface Specification," tech. rep., Aug 2013.

[12] L. Ding, G. Zhou, D. Morgan, Z. Ma, J. Kenney, J. Kim, and C. Giardina, "A robust digital baseband predistorter constructed using memory polynomials," *Communications, IEEE Transactions on*, vol. 52, pp. 159–165, Jan 2004.

[13] MATLAB, "Memoryless nonlinearity." http://http://www.mathworks.com/help/comm/ref/memorylessnonlinearity.html, October 2015.

[14] J. H. Lee, S. H. Cho, K. H. Doo, S. I. Myong, J. H. Lee, and S. S. Lee, "Cpri transceiver for mobile front-haul based on wavelength division multiplexing," in *ICT Convergence (ICTC), 2012 International Conference on*, pp. 581–582, Oct 2012.

[15] C. L. I, J. Huang, R. Duan, C. Cui, J. Jiang, and L. Li, "Recent progress on c-ran centralization and cloudification," *IEEE Access*, vol. 2, pp. 1030–1039, 2014.

[16] M. A. Marotta, N. Kaminski, I. Gomez-Miguelez, L. Z. Granville, J. Rochol, L. DaSilva, and C. B. Both, "Resource sharing in heterogeneous cloud radio access networks," *IEEE Wireless Communications*, vol. 22, pp. 74–82, June 2015.

[17] M. Paolini, "Beyond data caps. an analysis of the uneven growth in data traffic," *Senza Fili Consulting*, 2011.

[18] X. Wang, S. Thota, M. Tornatore, S.-S. Lee, H. H. Lee, S. Park, and B. Mukherjee, "Handover reduction via mobility-prediction-based vpon formation in optical-access-enabled cloud-ran," in *Optical Fiber Communications Conference and Exhibition (OFC), 2015*, pp. 1–3, March 2015.

[19] M. Qian, W. Hardjawana, J. Shi, and B. Vucetic, "Baseband processing units virtualization for cloud radio access networks," *IEEE Wireless Communications Letters*, vol. 4, pp. 189–192, April 2015.

[20] K. Boulos, M. E. Helou, and S. Lahoud, "Rrh clustering in cloud radio access networks," in *Applied Research in Computer Science and Engineering (ICAR), 2015 International Conference on*, pp. 1–6, Oct 2015.

[21] 3GPP, "Radio interface protocol architecture (3gpp ts 25.301 v6.4.0 (2005-09))."

[22] R. Wang, H. Hu, and X. Yang, "Potentials and challenges of c-ran supporting multi-rats toward 5g mobile networks," *IEEE Access*, vol. 2, pp. 1187–1195, 2014.

[23] 3GPP, "General packet radio service (gprs) enhancements for evolved universal terrestrial radio access network (e-utran) access (3gpp ts 23.401 v10.4.0 (2011-06))."

[24] D. Naboulsi, *Analysis and exploitation of mobile traffic datasets*. PhD thesis, Networking and Internet Architecture [cs.NI]. INSA Lyon, 2015. English. (tel-01235304v2).

[25] GNU, "Network simulator version 3.24." http://www.nsnam.org/, June 2016.

[26] M. Lacage, "Constant speed propagation delay model." http://www.nsnam.org/doxygen/propagation-delay-model_8h.html, June 2014.

[27] M. Lacage, "Random walk2d mobility model." http://www.nsnam.org/doxygen/random-walk-2d-mobility-model_8h.html, June 2014.

[28] M. Lacage, "Friis propagation loss model." http://www.nsnam.org/doxygen/friis-spectrum-propagation-loss_8cc_source.html, May 2016.

[29] B. Herman, "A3 rsrp handover algorithm." http://www.nsnam.org/doxygen/a3-rsrp-handover-algorithm_8cc_source.html, May 2016.

[30] L. N. Tran, E. K. Hong, and H. Liu, "A frequency domain equalization algorithm for fast time-varying fading channels," *Journal of Communications and Networks*, vol. 11, pp. 474–480, Oct 2009.

[31] M. Heck, "Grating coupler enabled optical isolators and circulators for photonic integrated circuits," *Selected Topics in Quantum Electronics, IEEE Journal of*, vol. 21, pp. 361–369, July 2015.

[32] Z. Yu, J. Teng, X. Bai, D. Xuan, and W. Jia, "Connected coverage in wireless networks with directional antennas," in *INFOCOM, 2011 Proceedings IEEE*, pp. 2264–2272, April 2011.

[33] P. Kyritsi, D. Cox, R. Valenzuela, and P. Wolniansky, "Effect of antenna polarization on the capacity of a multiple element system in an indoor environment," *Selected Areas in Communications, IEEE Journal on*, vol. 20, pp. 1227–1239, Aug 2002.

[34] R. Yuen, X. Fernando, and S. Krishnan, "Radio over multimode fiber for wireless access," in *Electrical and Computer Engineering, 2004. Canadian Conference on*, vol. 3, pp. 1715–1718 Vol.3, May 2004.

[35] A. Hekkala, M. Lasanen, L. Vieira, N. Gomes, and A. Nkansah, "Architectures for joint compensation of rof and pa with nonideal feedback," in *Vehicular Technology Conference (VTC 2010-Spring), 2010 IEEE 71st*, pp. 1–5, May 2010.

[36] J. Schaffner and W. Bridges, "Intermodulation distortion in high dynamic range microwave fiber-optic links with linearized modulators," *Lightwave Technology, Journal of*, vol. 11, pp. 3–6, Jan 1993.

[37] MATLAB, "Rf impairments library, version 8.5.0.197613 (r2015a)," in *The MathWorks Inc.*, 2015.

[38] L. Su and D. Chen, "Dynamic channel allocation schemes based on sinr analysis for cellular relaying networks," in *Computer Application and System Modeling (ICCASM), 2010 International Conference on*, vol. 13, pp. V13–104–V13–108, 2010.

[39] M. Petrova, N. Olano, and P. Mahonen, "Balls and bins distributed load balancing algorithm for channel allocation," in *Wireless On-demand Network Systems and Services (WONS), 2010 Seventh International Conference on*, pp. 25–30, 2010.

[40] M. Lacage, "Log distance propagation loss model." http://www.nsnam.org/doxygen/propagation-loss-model_8h.html, June 2014.

[41] T. Fujisawa, J. Hasegawa, K. Tsuchie, T. Shiozawa, T. Fujita, T. Saito, and Y. Unekawa, "A single-chip 802.11a mac/phy with a 32-b risc processor," *IEEE Journal of Solid-State Circuits*, vol. 38, pp. 2001–2009, Nov 2003.

[42] A. Hekkala, M. Hiivala, M. Lasanen, J. Perttu, L. Vieira, N. Gomes, and A. Nkansah, "Predistortion of radio over fiber links: Algorithms, implementation, and measurements," *Circuits and Systems I: Regular Papers, IEEE Transactions on*, vol. 59, pp. 664–672, March 2012.

[43] A. Shah and B. Jalali, "Adaptive equalisation for broadband predistortion linearisation of optical transmitters," *Optoelectronics, IEE Proceedings*, vol. 152, pp. 16–32, Feb 2005.

[44] A. Hekkala and M. Lasanen, "Performance of adaptive algorithms for compensation of radio over fiber links," in *Wireless Telecommunications Symposium, 2009. WTS 2009*, pp. 1–5, April 2009.

[45] J. Vuolevi, T. Rahkonen, and J. Manninen, "Measurement technique for characterizing memory effects in rf power amplifiers," *Microwave Theory and Techniques, IEEE Transactions on*, vol. 49, pp. 1383–1389, Aug 2001.

[46] S. Boumaiza and F. Ghannouchi, "Thermal memory effects modeling and compensation in rf power amplifiers and predistortion linearizers," *Microwave Theory and Techniques, IEEE Transactions on*, vol. 51, pp. 2427–2433, Dec 2003.

[47] R. Raich, H. Qian, and G. Zhou, "Orthogonal polynomials for power amplifier modeling and predistorter design," *Vehicular Technology, IEEE Transactions on*, vol. 53, pp. 1468–1479, Sept 2004.

[48] R. C. Johnson, *Antenna Engineering Handbook*. McGraw-Hill, Inc., 1993.

[49] G. Giannattasio, J. Erfanian, K. D. Wong, P. Wills, H. Nguyen, T. Croda, K. Rauscher, X. Fernando, and N. Pavlidou, *A Guide to the Wireless Engineering body of Knowledge*, ch. Radio frequency engineering, propagation and antennas, p. 141. A John Wiley & Sons, Ltd., Publication, 2009.